Published for SISSA by Springer

Received: *July 5, 2022*
Accepted: *November 20, 2022*
Published: *July 10, 2023*

# Measurement of the top quark pole mass using $\mathrm{t\bar{t}}$+jet events in the dilepton final state in proton-proton collisions at $\sqrt{s} = 13\,\mathrm{TeV}$

## The CMS collaboration

*E-mail:* cms-publication-committee-chair@cern.ch

Abstract: A measurement of the top quark pole mass $m_{\mathrm{t}}^{\mathrm{pole}}$ in events where a top quark-antiquark pair ($\mathrm{t\bar{t}}$) is produced in association with at least one additional jet ($\mathrm{t\bar{t}}$+jet) is presented. This analysis is performed using proton-proton collision data at $\sqrt{s} = 13\,\mathrm{TeV}$ collected by the CMS experiment at the CERN LHC, corresponding to a total integrated luminosity of $36.3\,\mathrm{fb}^{-1}$. Events with two opposite-sign leptons in the final state ($\mathrm{e}^{+}\mathrm{e}^{-}$, $\mu^{+}\mu^{-}$, $\mathrm{e}^{\pm}\mu^{\mp}$) are analyzed. The reconstruction of the main observable and the event classification are optimized using multivariate analysis techniques based on machine learning. The production cross section is measured as a function of the inverse of the invariant mass of the $\mathrm{t\bar{t}}$+jet system at the parton level using a maximum likelihood unfolding. Given a reference parton distribution function (PDF), the top quark pole mass is extracted using the theoretical predictions at next-to-leading order. For the ABMP16NLO PDF, this results in $m_{\mathrm{t}}^{\mathrm{pole}} = 172.93 \pm 1.36\,\mathrm{GeV}$.

Keywords: Hadron-Hadron Scattering , Top Physics

ArXiv ePrint: 2207.02270



https://doi.org/10.1007/JHEP07(2023)077

JHEP07(2023)077

## Contents



JHEP07(2023)077

## 1 Introduction

The top quark is the most massive elementary particle known. Its mass $m_t$ is a free parameter of the standard model (SM) Lagrangian and is an input to the global electroweak fits [1–4] and calculations of the Higgs boson self-coupling [5, 6]. The value of $m_t$ needs to be determined experimentally. Direct measurements of $m_t$ at hadron colliders, being dominated by measurements in proton-proton (pp) collisions at the CERN LHC, reach a precision on the order of 0.5 GeV [7–14]. The combined value of measurements by the CMS Collaboration at $\sqrt{s} = 7$ and 8 TeV is $m_t = 172.44 \pm 0.48$ GeV [10]. The direct measurements rely on the reconstruction of the top quark kinematic variables from its decay products and hence on the modeling provided by multipurpose Monte Carlo (MC) event generators. These generators typically make use of parton shower models to approximate higher-order effects, while heuristic models tuned to the data are used to describe the color

neutralization in the nonperturbative regime and the underlying event (UE). This introduces ambiguities in the interpretation of the top quark mass assumed in the simulation, $m_{\mathrm{t}}^{\mathrm{MC}}$. An additional intrinsic uncertainty on the order of about 0.5–1 GeV is expected when interpreting a direct measurement of $m_{\mathrm{t}}^{\mathrm{MC}}$ in terms of the top quark pole mass, $m_{\mathrm{t}}^{\mathrm{pole}}$ [15–22].

Alternatively, the value of $m_{\mathrm{t}}$ can be extracted by comparing cross section measurements to fixed-order theoretical predictions in well-defined renormalization schemes. The value of $m_{\mathrm{t}}^{\mathrm{pole}}$ was measured by both the ATLAS and CMS Collaborations [23–29], reaching an uncertainty below 1 GeV in a recent CMS measurement [29] by using the multidifferential cross sections of top quark-antiquark ($\mathrm{t\bar{t}}$) pair production. The top quark mass defined in the modified minimal subtraction ($\overline{\mathrm{MS}}$) scheme, referred to as the top quark running mass, was also measured [22, 30, 31] and its energy scale dependence was investigated in ref. [32].

In this paper, the value of $m_{\mathrm{t}}^{\mathrm{pole}}$ is measured by using the normalized differential cross section of $\mathrm{t\bar{t}}$ production in association with at least one energetic jet ($\mathrm{t\bar{t}}$+jet) [33]. The measurement follows the approach developed in refs. [31, 33, 34], where the normalized differential $\mathrm{t\bar{t}}$+jet cross section is measured as a function of the $\rho$ observable, defined as

$$\rho = \frac{2m_0}{m_{\mathrm{t\bar{t}+jet}}}, \tag{1.1}$$

where $m_{\mathrm{t\bar{t}+jet}}$ is the invariant mass of the $\mathrm{t\bar{t}}$+jet system. The result of the measurement does not depend on the choice of the scaling constant $m_0$, which is set to $m_0 = 170$ GeV, as used in previous measurements. The sensitivity to $m_{\mathrm{t}}$ is enhanced as compared to $\mathrm{t\bar{t}}$ production due to the presence of an additional jet because the kinematic parameters of the radiated gluons in $\mathrm{t\bar{t}}$+jet events depend on the mass of the top quark. High sensitivity to $m_{\mathrm{t}}^{\mathrm{pole}}$ is expected close to the production threshold, for $\rho > 0.65$, while for high $m_{\mathrm{t\bar{t}+jet}}$, e.g., $\rho < 0.55$, this sensitivity is small. Such a measurement was performed by the ATLAS Collaboration using pp collision data at $\sqrt{s} = 7$ and 8 TeV [26, 35], corresponding to integrated luminosities of 4.6 and 20.2 $\mathrm{fb}^{-1}$, respectively, finding a value of $m_{\mathrm{t}}^{\mathrm{pole}} = 171.1\,^{+1.2}_{-1.0}$ GeV with the 8 TeV data set.

In this paper, a measurement of $m_{\mathrm{t}}^{\mathrm{pole}}$ is made by using the $\rho$ dependence at the center-of-mass energy of 13 TeV. The data were recorded by the CMS detector in 2016, corresponding to an integrated luminosity of 36.3 $\mathrm{fb}^{-1}$.

In this analysis, the normalized differential cross section is measured at the detector level and is unfolded to the parton level. The unfolding is performed via the maximum likelihood method with profiled nuisance parameters for all systematic uncertainties, following the approach developed in ref. [32]. The signal and background processes are fitted simultaneously, and the systematic uncertainties and their correlations are determined from data. This leads to significantly improved experimental precision over classical approaches where systematic uncertainties are not profiled [22].

The paper is structured as follows. After a brief description of the CMS experiment and the event reconstruction in section 2, the data sets and simulation are presented in section 3, together with the definition of the signal. The event selection is explained in



JHEP07(2023)077

section 4. In section 5, a detailed description of multivariate analysis techniques developed for this measurement is given. The maximum likelihood fit for the signal extraction and unfolding is described in section 6, followed by a discussion of the systematic uncertainties in section 7. The determination of $m_{\mathrm{t}}^{\mathrm{pole}}$ is presented in section 8, and a summary is given in section 9. Tabulated results are provided in the HEPData record for this analysis [36].

## 2 The CMS detector and event reconstruction

The central feature of the CMS apparatus is a superconducting solenoid of 6 m internal diameter, providing a magnetic field of 3.8 T. Within the solenoid volume are a silicon pixel and strip tracker, a lead tungstate crystal electromagnetic calorimeter (ECAL), and a brass and scintillator hadron calorimeter (HCAL), each composed of a barrel and two endcap sections. Forward calorimeters extend the pseudorapidity ($\eta$) coverage provided by the barrel and endcap detectors. Muons are detected in gas-ionization chambers embedded in the steel flux-return yoke outside the solenoid. Events of interest are selected using a two-tiered trigger system. The first level (L1), composed of custom hardware processors, uses information from the calorimeters and muon detectors to select events at a rate of around 100 kHz within a fixed latency of about 4 $\mu$s [37]. The second level, known as the high-level trigger (HLT), consists of a farm of processors running a version of the full event reconstruction software optimized for fast processing, and reduces the event rate to around 1 kHz before data storage [38]. A more detailed description of the CMS detector, together with a definition of the coordinate system used and the relevant kinematic variables, can be found in ref. [39].

The primary vertex (PV) is taken to be the vertex corresponding to the hardest scattering in the event, evaluated using tracking information alone, as described in section 9.4.1 of ref. [40].

The particle-flow (PF) algorithm [41] aims to reconstruct and identify each individual particle in an event, with an optimized combination of information from the various elements of the CMS detector. The energy of photons is obtained from the ECAL measurement. The energy of electrons is determined from a combination of the electron momentum at the PV as determined by the tracker, the energy of the corresponding ECAL cluster, and the energy sum of all bremsstrahlung photons spatially compatible with originating from the electron track. The energy of muons is obtained from the curvature of the corresponding track. The energy of charged hadrons is determined from a combination of their momentum measured in the tracker and the matching ECAL and HCAL energy deposits, corrected for the response function of the calorimeters to hadronic showers. Finally, the energy of neutral hadrons is obtained from the corresponding corrected ECAL and HCAL energies.

For each event, hadronic jets are clustered from PF particles using the infrared- and collinear-safe anti-$k_{\mathrm{T}}$ algorithm with a distance parameter of 0.4. Jet momentum is determined as the vectorial sum of all particle momenta in the jet, and is found from simulation to be, on average, within 5 to 10% of the true momentum over the whole transverse momentum ($p_{\mathrm{T}}$) spectrum and detector acceptance. Additional pp interactions within the



JHEP07(2023)077

same or nearby bunch crossings (pileup) can contribute additional tracks and calorimetric energy depositions, increasing the apparent jet momentum. To mitigate this effect, tracks identified to be originating from pileup vertices are discarded and an offset correction is applied to correct for remaining contributions. Jet energy corrections are derived from simulation studies so that the average measured energy of jets becomes identical to that of particle-level jets. In situ measurements of the momentum balance in dijet, photon+jet, Z+jet, and multijet events are used to determine any residual differences between the jet energy scale in data and in simulation, and appropriate corrections are made [42]. No dedicated flavor-dependent corrections are made. Additional selection criteria are applied to each jet to remove jets potentially dominated by instrumental effects or reconstruction failures. The jet energy resolution amounts typically to 15–20% at 30 GeV, 10% at 100 GeV, and 5% at 1 TeV, and corrections as determined from QCD dijet and $\gamma$+jet events [42] are applied.

The missing transverse momentum vector $\vec{p}_{\mathrm{T}}^{\,\mathrm{miss}}$ is computed as the negative vector sum of the $\vec{p}_{\mathrm{T}}$ of all the PF candidates in an event, and its magnitude is denoted as $p_{\mathrm{T}}^{\mathrm{miss}}$ [43]. The value of $\vec{p}_{\mathrm{T}}^{\,\mathrm{miss}}$ is modified to account for corrections to the energy scale of the reconstructed jets in the event. A pileup per particle identification algorithm [44, 45] is applied to reduce the pileup dependence of $\vec{p}_{\mathrm{T}}^{\,\mathrm{miss}}$ and the PF candidates are weighted by their probability to originate from the PV [43].

Electrons are measured in the range $|\eta| < 2.5$, and the single-electron trigger efficiency is about 80%. The electron momenta are estimated by combining energy measurements in the ECAL with momentum measurements in the tracker [46]. The efficiency to reconstruct and identify electrons is better than 95% [47]. The momentum resolution for electrons with $p_{\mathrm{T}} \approx 45$ GeV from $\mathrm{Z} \to \mathrm{ee}$ decays ranges from 1.6 to 5%. It is generally better in the barrel region ($|\eta| < 1.479$) than in the endcaps ($1.479 < |\eta| < 3.0$), and also depends on the bremsstrahlung energy emitted by the electron as it traverses the material in front of the ECAL [46, 47].

Muons are measured in the range $|\eta| < 2.4$, with detection planes made using three technologies: drift tubes, cathode strip chambers, and resistive plate chambers. The single-muon trigger efficiency exceeds 90% over the full $\eta$ range, and the efficiency to reconstruct and identify muons is greater than 96%. Matching muons to tracks measured in the silicon tracker results in a relative $p_{\mathrm{T}}$ resolution, for muons with $p_{\mathrm{T}}$ up to 100 GeV, of 1% in the barrel and 3% in the endcaps. The $p_{\mathrm{T}}$ resolution in the barrel is better than 7% for muons with $p_{\mathrm{T}}$ up to 1 TeV [48].

## 3 Data samples and event simulation

The analysis uses pp collision data recorded by the CMS experiment in 2016, corresponding to an integrated luminosity of 36.3 $\mathrm{fb}^{-1}$. The events are required to pass one of several HLT selection criteria, including the presence of either one or two leptons (electrons or muons). The single-electron (muon) trigger requires a minimum $p_{\mathrm{T}}$ of 27 (24) GeV. In the case of the dielectron triggers, at least two lepton candidates with a minimum $p_{\mathrm{T}}$ of 23 and 12 GeV are required, while for the dimuon triggers the respective thresholds are 17 and



JHEP07(2023)077

8 GeV. For the electron-muon triggers, the selection requirements are $p_T > 23$ GeV and $p_T > 8$ GeV ($p_T > 13$ GeV) if the muon (electron) is the lepton with higher $p_T$.

Signal and background $t\bar{t}$ processes are simulated using the POWHEG (version 2) [49–51] MC generator at next-to-leading order (NLO) in quantum chromodynamics (QCD) for the matrix element (ME) calculations. The top quark mass in the simulation is fixed to $m_t^{MC} = 172.5$ GeV and the proton structure is described using the NNPDF 3.1 PDF at next-to-NLO (NNLO) [52, 53]. Parton showering is performed using PYTHIA (version 8.230) [54] with the CP5 tune [55]. The $h_{damp}$ parameter in POWHEG, which effectively regulates the matching scale to the parton shower, is set to $h_{damp} = 1.379 m_t^{MC}$ [55]. The $t\bar{t}$ simulation is split into different components, modeling the signal and the background contributions, as described in section 3.1.

Additionally, simulated samples of the $t\bar{t}$ process are generated with up to two extra partons at the NLO ME level using MADGRAPH5_aMC@NLO [56]. These are used to derive the calibrations of the neural networks (NNs), as discussed in section 5. Events are matched using the FxFx [57] prescription to the PYTHIA parton shower, while MADSPIN [58] is used to model the decays of the top quark and antiquark at leading order (LO). The matching scale for the MADGRAPH5_aMC@NLO [FxFx] sample is set to 40 GeV.

The background contributions arise from single top quark production in association with a W boson (tW), $Z/\gamma^*$ or W bosons produced with additional jets (Z+jets, W+jets), and diboson production (WW, WZ, ZZ). The contributions from the diboson and W+jets production processes are labeled as "Other" in the figures. For all the background samples, PYTHIA is used to model the parton showering, hadronization, and multiparton interactions. The tW process is simulated using POWHEG [59, 60] at NLO with the same tune and modeling parameters as used for the $t\bar{t}$ process. The CUETP8M1 [61–63] tune is used for the background simulation. The Z+jets process is simulated using MADGRAPH5_aMC@NLO at LO with up to four additional partons at ME level, and is matched to the PYTHIA parton shower using the MLM [64, 65] prescription. Similarly, W+jets samples are produced using MADGRAPH5_aMC@NLO at LO with up to four additional partons at ME level. To derive the NN calibrations, an independent Z+jets simulation is generated with MADGRAPH5_aMC@NLO at NLO using the FxFx merging prescription. Diboson production is simulated at LO with PYTHIA.

All predictions are normalized to their theoretical cross section and the corresponding integrated luminosity of the data set. For the $t\bar{t}$ signal, the value of the cross section is $830.91\,^{+20.39}_{-29.96}$ (scale) $^{+3.92}_{-3.83}$ (PDF+$\alpha_S$) pb, as calculated with the TOP++ (version 2.0) program [66] at NNLO precision. The calculation assumes $m_t = 172.5$ GeV, makes use of the NNPDF3.1 PDF set at NNLO, and includes the resummation of next-to-next-to-leading-logarithmic soft-gluon terms [67–72]. The labels "scale" and $\alpha_S$ refer to the uncertainty assessed by varying the renormalization ($\mu_R$) and factorization ($\mu_F$) scales and the value for the strong coupling constant, respectively. The remaining cross sections are calculated at approximate NNLO for tW production [73], NLO for Z+jets and diboson production [74], and NNLO for W+jets [75] production.

For all simulated samples, the CMS detector response is simulated with GEANT4 [76]. To model the effect of pileup, additional minimum-bias interactions are added to the



JHEP07(2023)077

simulated events. Weights are used with the simulated events to reproduce the pileup distribution in the data. The weights are estimated from the measured bunch-to-bunch instantaneous luminosity, assuming a total inelastic pp cross section of 69.2 mb [77].

### 3.1 Signal definition at the parton level

The simulated signal consists of $\mathrm{t\bar{t}}$ events in which a dilepton and at least one jet emitted at the parton level with $p_{\mathrm{T}} > 30\,\mathrm{GeV}$ and $|\eta| < 2.4$ are produced. The parton level is defined after parton showering with on-shell top quarks. Additional jets are clustered by applying the anti-$k_{\mathrm{T}}$ algorithm [78, 79] with a distance parameter of 0.4, using all particles before hadronization that do not stem from the top quark decays. The $\mathrm{t\bar{t}}$+jet signal is obtained from the nominal $\mathrm{t\bar{t}}$ simulation by selecting events with at least one additional parton-level jet passing the selection described above. The remaining events are considered as background and labeled as $\mathrm{t\bar{t}}$+0 jet. The $\mathrm{t\bar{t}}$+jet signal is further split into subprocesses that are defined based on the value of $\rho$ at parton level in the following binning: 0–0.3, 0.3–0.45, 0.45–0.7, and 0.7–1. The binning choice is explained in section 6. The simulated $\mathrm{t\bar{t}}$ signal demands at least two leptons, including those from the decays of tau leptons. The remaining $\mathrm{t\bar{t}}$ events are considered as background. The unfolded results are extrapolated to the full phase space using the $\mathrm{t\bar{t}}$ MC simulation.

## 4 Event selection

Data events containing two opposite-sign leptons ($\mathrm{e^+e^-}$, $\mu^+\mu^-$, $\mathrm{e^\pm}\mu^\mp$) are selected. To suppress events from low-mass resonance decays and the Drell-Yan process, the dilepton invariant mass ($m_{\ell\ell}$) is required to be larger than 20 GeV. The Z+jets background contribution is reduced by discarding events with $p_{\mathrm{T}}^{\mathrm{miss}} < 40\,\mathrm{GeV}$ and $m_{\ell\ell}$ in the Z mass window between 76 and 106 GeV, for the same-flavor lepton channels.

The leading (subleading) electron candidate is required to have $p_{\mathrm{T}} > 25$ (20) GeV and $|\eta| < 2.4$. Electrons reconstructed in the ECAL barrel-endcap transition region ($1.44 < |\eta| < 1.57$) are rejected. A relative isolation parameter ($I_{\mathrm{rel}}$) is calculated for each electron candidate, defined as the ratio of the $p_{\mathrm{T}}$ sum of neutral and charged hadron and photon PF candidates, within a distance of $\Delta R = \sqrt{(\Delta\eta)^2 + (\Delta\phi)^2} = 0.3$ in $\eta$-$\phi$ space, to the $p_{\mathrm{T}}$ of the electron candidate, where $\phi$ is the azimuthal angle. Depending on the electron $p_{\mathrm{T}}$, the maximum allowed value for $I_{\mathrm{rel}}$ varies from 0.05 to 0.1. Additional corrections are made to remove contributions from pileup [47]. To reject misidentified electron candidates and photon conversions, additional identification requirements are imposed [47].

Muon candidates are selected with the same $p_{\mathrm{T}}$ and $\eta$ requirements as for the electrons, except for removing the transition-region requirement. An isolation requirement of $I_{\mathrm{rel}} < 0.15$ is applied, where all particle momenta within a distance of $\Delta R < 0.4$ from the muon are considered and pileup effects are taken into account. Muon candidates are further identified by their specific signature in the detector [48].

Jets with $p_{\mathrm{T}} > 30\,\mathrm{GeV}$ and $|\eta| < 2.4$ are selected, and the value of $\Delta R$ between the jet and the selected lepton candidates must be greater than 0.4. To further reject jets arising from pileup interactions, a dedicated pileup jet identification algorithm [45] is employed



JHEP07(2023)077

for jets with $p_T$ between 30 and 50 GeV. Jets originating from the hadronization of b quarks (called b jets) are identified (tagged) using the DeepCSV algorithm [80], which makes use of associated track and secondary-vertex information as inputs to a deep NN. The chosen operating point for the discriminator has an efficiency of about 80–90% for b jets, for misidentification ("mistag") rates of 10 and 40% for light-quark and c quark jets, respectively [80]. The energy measurement of b jets is improved by about 6–12% using a deep NN estimator [81].

Lepton trigger and identification efficiencies, lepton momentum resolutions, and b tagging efficiencies are corrected in simulation to match the values in data.

The typical purities for the $t\bar{t}$+jet signal obtained without requirements on the jet or b jet multiplicity range from about 15% in the $e^+e^-$ and $\mu^+\mu^-$ channels to about 30% in the $e^\pm\mu^\mp$ channel. When selecting only events with at least three reconstructed jets, of which one is b tagged, the purity is around 75%.

Figures 1 and 2 show the distributions of several kinematic observables from data and simulation for the combined dilepton candidates. In general, the MC simulation describes the data well. A small discrepancy between the normalization of the data and simulation is observed in several of the distributions. However, this does not affect this measurement since the normalization is determined from the likelihood fit, as described in section 6, and the normalized cross section is used to extract $m_t^{pole}$. Some trends can be observed in the jet and lepton momentum distributions, where the spectrum predicted by the simulation has a higher average value than the one observed in data. The effect is related to the modeling of the top quark $p_T$ in the POWHEG+PYTHIA8 $t\bar{t}$ simulation, and similar observations have been made in previous measurements [82–85] when comparing the measured distributions to detector- or particle-level predictions. The jet multiplicity and b jet multiplicities from data are well described by the simulation within the total uncertainties.

## 5 Multivariate analysis

To reconstruct $\rho$ as the variable of interest, kinematic reconstruction techniques must be employed. These methods typically rely on imposing constraints to reconstruct the longitudinal components of the momenta of the two neutrinos from the W boson leptonic decays in $t\bar{t}$ events containing dileptons. Several methods have been established and used in previous differential $t\bar{t}$ cross section measurements [29, 32, 82–86].

Two multivariate analysis (MVA) approaches are developed to mitigate constraints on the kinematic reconstruction and and improve the signal-versus-background discrimination. The MVA methods developed for this analysis are described below.

### 5.1 Reconstruction of top quark kinematic variables

Two analytical kinematic reconstruction approaches referred to as "full kinematic reconstruction" and "loose kinematic reconstruction" are used. Solutions of both methods are considered as inputs to the MVAs. For the full kinematic reconstruction, the four-momenta of the top quark and antiquark are determined using the following constraints: total $\vec{p}_T$ conservation; the mass of the W boson (80.4 GeV), and the masses of the top quark and



JHEP07(2023)077

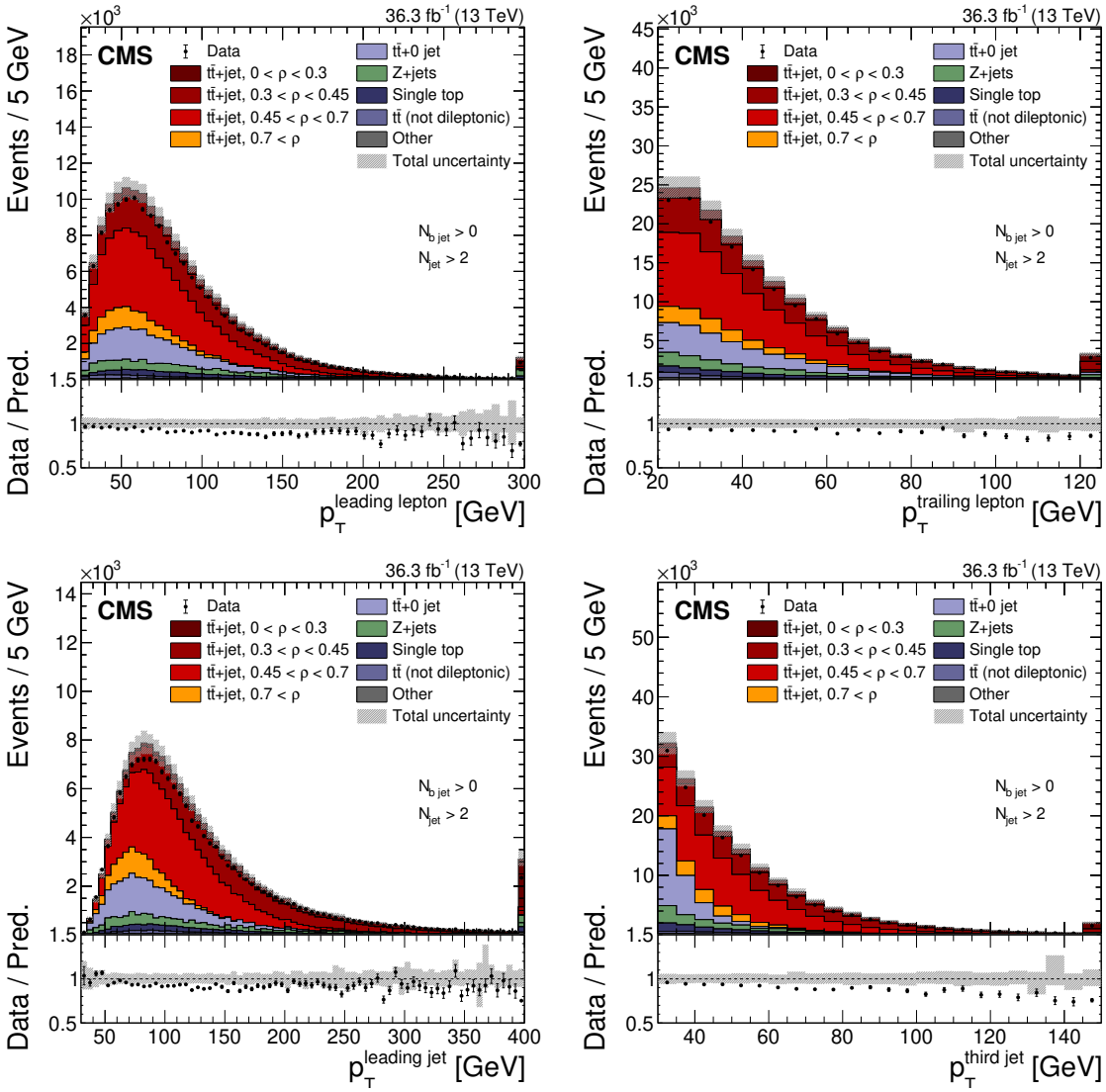


**Figure 1**. The observed (points) and predicted (stacked histograms) signal and background yields as a function of the leading (upper left) and subleading (upper right) lepton $p_{\mathrm{T}}$ and leading (lower left) and third-highest (lower right) jet $p_{\mathrm{T}}$ after applying the signal selection. The vertical bars on the points represent the statistical uncertainty in the data. The hatched band represents the total uncertainty in the sum of the simulated signal and background predictions. The lower panels show the ratio of the data to the sum of the signal and background predictions.

antiquark (172.5 GeV). Reconstructed $\vec{p}_{\mathrm{T}}^{\,\mathrm{miss}}$ in the event is assumed to originate from the two neutrinos produced in the two W boson decays. Possible ambiguities in the algebraic solutions are solved by taking the solution with the smallest $\mathrm{t\bar{t}}$ invariant mass. To increase the reconstruction efficiency and account for the detector resolution, the reconstruction procedure is repeated 100 times for each event. Each time, reconstructed momenta of the measured jets and leptons are randomly smeared according to their resolution, where the smearing effect is propagated to $\vec{p}_{\mathrm{T}}^{\,\mathrm{miss}}$. Each of the 100 solutions is weighted based on the



JHEP07(2023)077

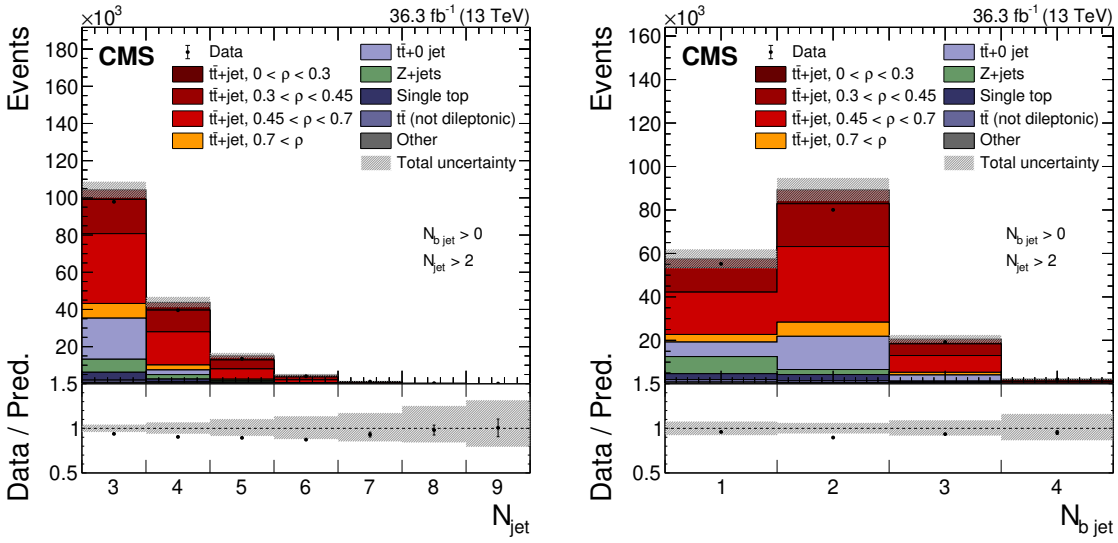


**Figure 2**. The observed (points) and predicted (stacked histograms) signal and background yields as a function of the jet (left), and b jet (right) multiplicities, after applying the signal selection. The vertical bars on the points represent the statistical uncertainty in the data. The hatched band represents the total uncertainty in the sum of the simulated signal and background predictions. The lower panels show the ratio of the data to the sum of the signal and background predictions.

true distribution of the invariant mass of a lepton and a b jet ($m_{\ell \mathrm{b}}$) stemming from the top quark decays as given by the simulation, where the weights for both decay chains of the t and $\overline{\mathrm{t}}$ are multiplied. All combinations of jets and leptons with $m_{\ell \mathrm{b}} < 180\,\mathrm{GeV}$ are considered and ranked by the presence of b jets in the solutions, where solutions with a higher b jet multiplicity are preferred. Further details about the reconstruction method can be found in ref. [82].

In the loose kinematic reconstruction [29], only the $\mathrm{t\bar{t}}$ system as a whole is reconstructed. The advantage of this method is that the $m_{\mathrm{t}}$ constraint is not used, which makes this method especially useful for the determination of $m_{\mathrm{t}}$. Similarly to the full kinematic reconstruction, only jet–lepton combinations with $m_{\ell \mathrm{b}} < 180\,\mathrm{GeV}$ are considered. Combinations based on the different assignments are ranked by the number of b jets, and solutions with more b jets are preferred. Among combinations with the same number of b jets, the one with the highest $p_{\mathrm{T}}$ jets are chosen. The kinematic variables of the $\nu\overline{\nu}$ system are obtained as follows: $\vec{p}_{\mathrm{T}}^{\,\nu\overline{\nu}}$ is set equal to $\vec{p}_{\mathrm{T}}^{\,\mathrm{miss}}$ and its longitudinal component and energy are set equal to that of the charged-lepton-pair system. Furthermore, constraints are imposed on the reconstructed invariant masses of the $\mathrm{W^+W^-}$, $m(\mathrm{W^+W^-}) > 2m_{\mathrm{W}}$, and neutrino pair, $m(\nu\overline{\nu}) > 0$.

To optimize the resolution of the $\rho$ observable, an MVA approach is developed, based on a regression NN, where the target variable is the parton-level $\rho$ as defined in the MC. Using the TensorFlow [87] package and the Keras [88] backend, a fully connected feed-forward NN is trained. An NN with two hidden layers of 512 nodes each is used. Low-level variables include basic event information such as the $p_{\mathrm{T}}$ of a reconstructed particle, whereas high-



JHEP07(2023)077

level variables include such things as the solutions to the kinematic reconstruction. Starting from a set of more than 100 low- and high-level input variables, the ten most relevant input variables are identified and selected, while the remaining ones are discarded. All events passing the selection described in section 4 and having at least three reconstructed jets are considered in the training. As introduced in section 3, a statistically independent training sample is obtained using $\mathrm{t\bar{t}}$ MC events simulated with the MadGraph5_aMC@NLO [FxFx] event generator interfaced with pythia8. All NN hyperparameters are optimized using a Bayesian optimizer approach [89–91], and the final NN response is cross-checked using the powheg+pythia8 simulation. Input variables, ordered by their impact, used for the regression NN are

- solution for $\rho$ using the loose kinematic reconstruction,
- solution for $\rho$ using the full kinematic reconstruction,
- invariant mass of the dilepton and subleading jet system,
- invariant mass of the leading lepton and subleading jet system,
- $p_{\mathrm{T}}$ of the subleading lepton,
- invariant mass of the dilepton,
- invariant mass of the subleading lepton and subleading jet system,
- invariant mass of the subleading lepton and leading jet system,
- invariant mass of the dilepton and leading jet system,
- $p_{\mathrm{T}}^{\mathrm{miss}}$.

If no solution from the kinematic reconstruction is obtained, a value of zero is used instead. The agreement between data and simulation for all inputs is evaluated using goodness-of-fit tests based on a saturated model [92]. All the input variables are found to have a $p$-value $> 0.08$, when compared between data and simulation. The test procedure and the final result are independent of the cross section and not sensitive to $m_{\mathrm{t}}$.

The performance of the NN regression is shown in figure 3, where the correlation between the parton-level $\rho$ value ($\rho_{\mathrm{true}}$) and the reconstructed value ($\rho_{\mathrm{reco}}$) is shown. The regression correlation coefficient is 0.87, compared to 0.78 (0.84) for the loose (full) kinematic reconstruction. In the same figure, the $\rho_{\mathrm{reco}}$ resolution of the obtained solutions is displayed as a function of $\rho_{\mathrm{true}}$. The $\rho_{\mathrm{reco}}$ resolution in each bin of $\rho_{\mathrm{true}}$ is defined as the root-mean-square of the difference between $\rho_{\mathrm{reco}}$ and $\rho_{\mathrm{true}}$, divided by $1 + \langle \rho_{\mathrm{true}} - \rho_{\mathrm{reco}} \rangle$. A resolution between 0.05–0.08 is obtained over the entire spectrum, which is a significant improvement compared to the two analytical reconstruction methods that have a resolution in the range 0.10–0.13 for $\rho_{\mathrm{true}} > 0.5$. Moreover, unlike the kinematic reconstruction methods, which are affected by reconstruction inefficiencies, the NN approach gives a measurement of $\rho$ for every event. In this analysis, the solution of the MVA regression is used, and is indicated with $\rho_{\mathrm{reco}}$. Distributions of $\rho_{\mathrm{reco}}$ for the data and simulation are shown in figure 4 for the $\mathrm{e}^{\pm}\mu^{\mp}$ (left plot) and same-flavor (right plot) dilepton channels.



JHEP07(2023)077

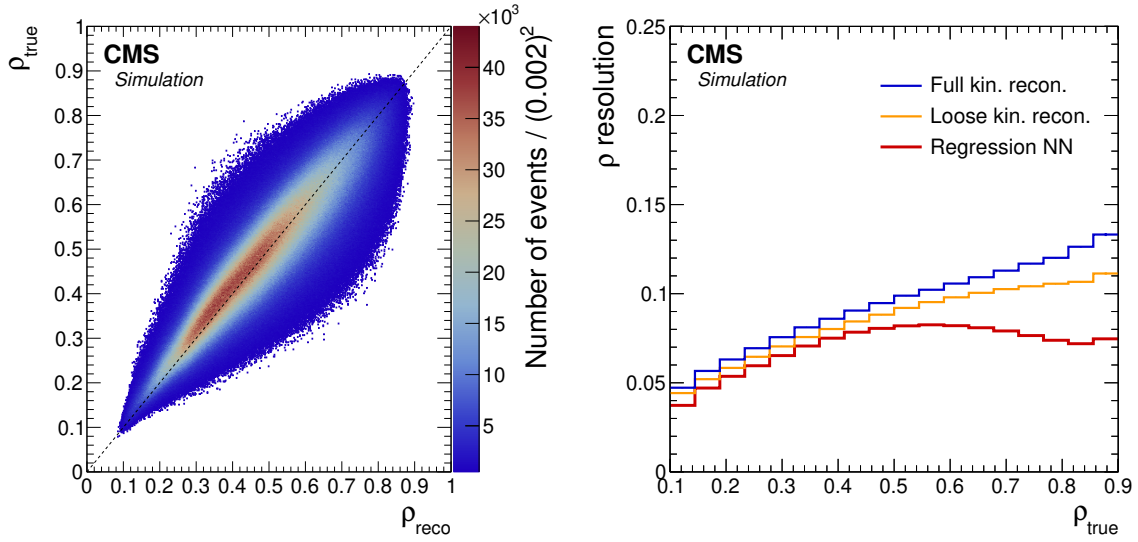


**Figure 3**. The correlation between $\rho_{\text{true}}$ and $\rho_{\text{reco}}$ is shown for the regression NN reconstruction method (left). The $\rho_{\text{reco}}$ resolution, defined in the text, as a function of $\rho_{\text{true}}$ (right) for the full (blue line) and loose (orange line) kinematic reconstructions and the regression NN (red line) methods. The number of events per bin in the left plot is shown by the color scale.

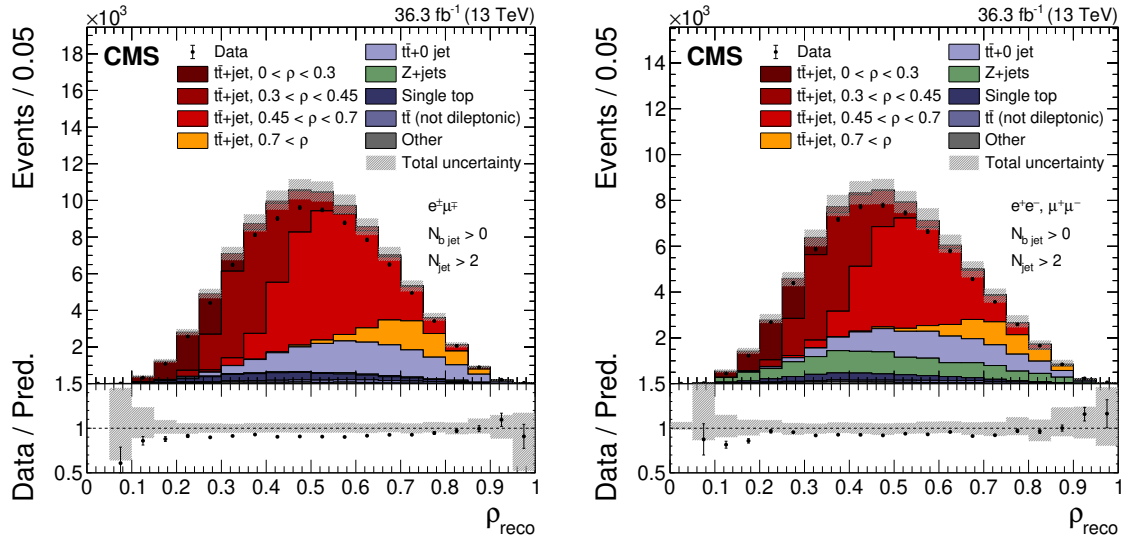


**Figure 4**. The observed (points) and MC predicted (stacked histograms) signal and background yields as a function of $\rho_{\text{reco}}$ as determined by the NN reconstruction method for the $e^{\pm}\mu^{\mp}$ (left) and same-flavor dilepton channels (right). The vertical bars on the points represent the statistical uncertainty in the data. The hatched band represents the total uncertainty in the sum of the simulated signal and background predictions. The lower panels show the ratio of the data to the sum of the signal and background predictions.

JHEP07(2023)077

### 5.2 Event classification

To maximize the signal sensitivity and increase the separation between the $t\bar{t}$+jet signal and Z+jets and $t\bar{t}$+0 jet backgrounds, an MVA event classifier is developed. Using the same interface as for the regression NN, a fully connected feed-forward event-classification NN is defined, with the same strategies for the input-variable selection and optimization. Independent sets of training samples are obtained by using the NLO MadGraph5_aMC@NLO [FxFx]+Pythia8 simulation for the $t\bar{t}$ and Z+jets events, which are not used in the likelihood fit. The input variables chosen for this NN, ranked by impact, are

- $p_T$ of the additional third jet beyond the two jets from the top quark decays, as determined in the solution of the full kinematic reconstruction,
- $p_T$ of the third-highest-$p_T$ jet,
- invariant mass of the dilepton system,
- $p_T^{miss}$,
- mass of the leading lepton,
- mass of the subleading lepton,
- $p_T$ of the leading jet,
- $p_T$ of the dilepton system,
- number of reconstructed jets,
- $p_T$ of the leading lepton.

The architecture of the classification network has three output nodes, corresponding to the three process classes ($t\bar{t}$+jet, Z+jets, and $t\bar{t}$+0 jet). The separation into multiple processes provides a better discrimination of the signal versus background events as compared to a binary-classifier approach. Because the response of the output nodes is used at a later step in the unfolding procedure (section 6), any bias in the obtained response with respect to the $\rho$ observable is reduced by making use of unsupervised domain adaptation by back propagation [93]. In this method, additional layers are added to the NN with the optimization target of regressing $\rho_{reco}$ as an ancillary output node, whereas the sign of the gradient in the back-propagation algorithm is inverted such that the NN does not learn to use input information sensitive to $\rho_{reco}$. The trained NN uses four hidden layers with 204 nodes each. The background rejection of the event-classification NN is shown in figure 5 by the distributions of the NN output scores for the $t\bar{t}$+jet signal $s(t\bar{t}$+jet) (left) and $t\bar{t}$+0 jet background $s(t\bar{t})$ (right) events from data and simulation.



JHEP07(2023)077

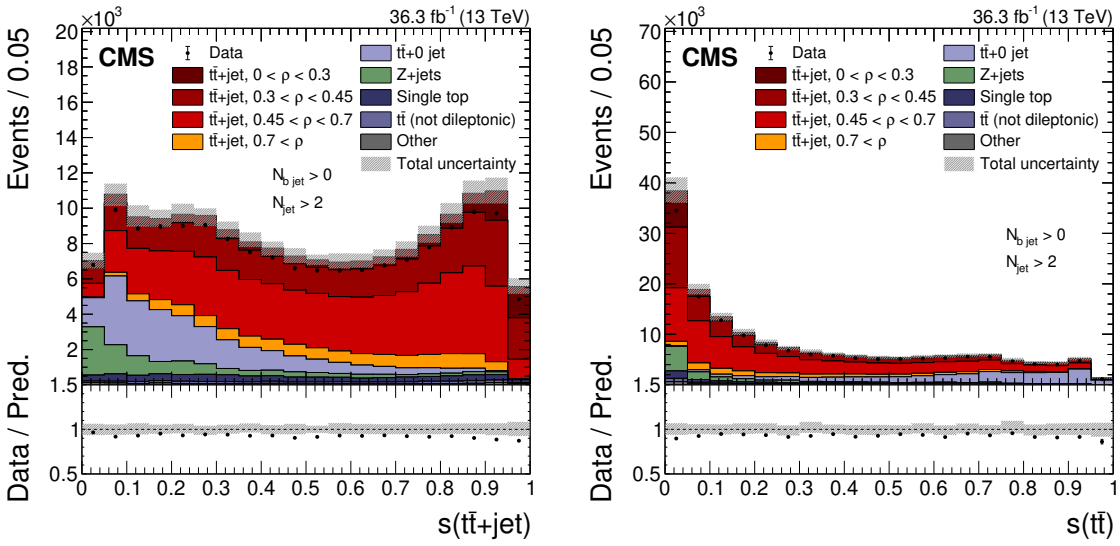


**Figure 5**. The observed (points) and MC predicted (stacked histograms) signal and background yields as a function of the signal (left) and $\mathrm{t\bar{t}}$+0 jet background (right) output node score of the classifier NN. The vertical bars on the points represent the statistical uncertainty in the data. The hatched band represents the total uncertainty in the sum of the simulated signal and background predictions. The lower panels show the ratio of the data to the sum of the signal and background predictions.

## 6 Signal extraction, cross section measurement, and unfolding

The differential cross section $\mathrm{d}\sigma_{\mathrm{t\bar{t}+jet}}/\mathrm{d}\rho$ is measured at the parton level in four $\rho$ bins using a maximum likelihood fit to final-state distributions, following the method of ref. [32]. Since this method allows us to deal with larger background contributions, looser selection requirements compared to other analyses can be imposed. This allows us to maximize the signal acceptance and hence minimize the extrapolation uncertainties. Systematic uncertainties are profiled in the likelihood function as nuisance parameters and are constrained using the data. The expected signal and background distributions and the effect of the systematic uncertainties are estimated using the MC simulations. The total cross section in each bin $k$ of the $\rho$ distribution, $\sigma^{k}_{\mathrm{t\bar{t}+jet}}$, is measured. This is related to the differential cross section $\mathrm{d}\sigma_{\mathrm{t\bar{t}+jet}}/\mathrm{d}\rho$ as

$$\sigma^{k}_{\mathrm{t\bar{t}+jet}} = \int_{\rho^{k}_{\mathrm{low}}}^{\rho^{k}_{\mathrm{high}}} \frac{\mathrm{d}\sigma_{\mathrm{t\bar{t}+jet}}}{\mathrm{d}\rho}\,\mathrm{d}\rho, \tag{6.1}$$

where $\rho^{k}_{\mathrm{low}}$ and $\rho^{k}_{\mathrm{high}}$ denote the lower and the upper bounds of the $k$-th generator-level bin in $\rho$, respectively.

The likelihood function $\mathcal{L}$ assumes that the number of observed events in each bin follows a Poisson distribution and can be written as:

$$\mathcal{L} = \prod_{i} \frac{\mathrm{e}^{-v_i} v_i^{n_i}}{n_i!} \prod_{j} \pi(w_j) \prod_{m} \pi(\lambda_m). \tag{6.2}$$



JHEP07(2023)077

Here, $i$ denotes the index of the bin in the final-state distribution, and $v_i$ and $n_i$ are the expected and observed number of events in bin $i$, respectively. The additional terms $\pi(w_j)$ and $\pi(\lambda_m)$ are the prior probability density functions (pdfs) for the normalization of each background process $w_j$ and nuisance parameter $\lambda_m$, respectively.

The expected number of events $v_i$ can be written as:

$$v_i = \sum_k s_i^k \left(\sigma^k_{\mathrm{t\bar{t}+jet}}, \vec{\lambda}, m_\mathrm{t}^\mathrm{MC}\right) + \sum_j b_i^j \left(w_j, \vec{\lambda}, m_\mathrm{t}^\mathrm{MC}\right), \tag{6.3}$$

where $s_i^k$ is the number of expected $\mathrm{t\bar{t}}$+jet signal events from the $k$-th generator-level bin for a reconstructed $\rho$ value in bin $i$. The value of $s_i^k$ depends on $\sigma^k_{\mathrm{t\bar{t}+jet}}$, the nuisance parameters $\vec{\lambda}$, and the top quark mass used in the simulation $m_\mathrm{t}^\mathrm{MC}$, which is needed to model the acceptance and extrapolate the results to the full phase space. Analogously, $b_i^j$ is the number of expected background events from process $j$, and depends on its normalization $w_j$, the nuisance parameters $\vec{\lambda}$, and on $m_\mathrm{t}^\mathrm{MC}$ in the case of the $\mathrm{t\bar{t}}$ and tW backgrounds.

Since $v_i$ implicitly incorporates the dependence of the parton-level cross section $\sigma^k_{\mathrm{t\bar{t}+jet}}$ on the experimental acceptance and detector response, the maximization of the likelihood function yields the results that are directly unfolded to the parton level.

For each cross section bin $k$, a signal strength parameter $r_k$ is assigned, defined as

$$r_k = \frac{\sigma^k_{\mathrm{t\bar{t}+jet}}}{\sigma^k_{\mathrm{t\bar{t}+jet}}(\mathrm{MC})}, \tag{6.4}$$

where the denominator is the cross section corresponding to the normalization of the MC simulation. In the fit, all the signal strength parameters are fitted simultaneously. The $\sigma^k_{\mathrm{t\bar{t}+jet}}(\mathrm{MC})$ values are determined using the nominal NLO POWHEG+PYTHIA8 simulation, and the nuisance parameters are constrained simultaneously with the differential cross section values.

To mitigate the correlation between the fitted signal strength parameters and $m_\mathrm{t}^\mathrm{MC}$, the latter is added as an additional free parameter to the fit. For this purpose, additional predictions are obtained from two dedicated MC simulations where the value of $m_\mathrm{t}^\mathrm{MC}$ is set to 169.5 or 175.5 GeV. In the simultaneous fit, the dependence of the measured $\sigma^k_{\mathrm{t\bar{t}+jet}}$ on $m_\mathrm{t}^\mathrm{MC}$ is fully taken into account. Therefore, the resulting $\mathrm{d}\sigma_{\mathrm{t\bar{t}+jet}}/\mathrm{d}\rho$ can be compared to the fixed-order calculations without assumptions on the relationship between $m_\mathrm{t}^\mathrm{MC}$ and $m_\mathrm{t}^\mathrm{pole}$ [94]. This method was proposed in refs. [25, 94] and was used in previous CMS measurements [22, 32]. The likelihood construction and the minimization of $-2\ln(\mathcal{L})$ using MINUIT [95] follows the procedures described in refs. [96–98], as does the estimation of the uncertainties using MINOS [95]. The nuisance parameters corresponding to the shape and normalization are modeled using Gaussian and log-normal prior pdfs, respectively, based on their input uncertainties before the fit to the data. The dependence of the templates on the nuisance parameters is interpolated quadratically (linearly) within (beyond) one standard deviation, as described in ref. [99]. The systematic uncertainty templates are built so as to reflect the variations found in estimating the systematic uncertainties.



JHEP07(2023)077

| | Reconstructed $\rho$ | | | | No reconstructed $\rho$ | |
|---|---|---|---|---|---|---|
| | $N_{\text{jet}} \geq 3$ | | | | $N_{\text{jet}} = 1$ | $N_{\text{jet}} = 2$ |
| | $\rho < 0.3$ | $0.3 < \rho < 0.45$ | $0.45 < \rho < 0.7$ | $\rho > 0.7$ | | |
| $N_{\text{b jet}} = 1$ | $R_{\text{NN}}$ | $R_{\text{NN}}$ | $R_{\text{NN}}$ | $R_{\text{NN}}$ | $p_{\text{T}}^{\text{leading jet}}$ | $p_{\text{T}}^{\text{subleading jet}}$ |
| $N_{\text{b jet}} \geq 2$ | $R_{\text{NN}}$ | $R_{\text{NN}}$ | $R_{\text{NN}}$ | $R_{\text{NN}}$ | — | $m_{\ell\text{b}}^{\text{min}}$ |

**Table 1**. A list of the event categories and distributions used in the maximum likelihood fit.

The measurement is performed in four bins of $\rho_{\text{true}}$ and $\rho_{\text{reco}}$: 0–0.3, 0.3–0.45, 0.45–0.7, and 0.7–1.0, where the bin boundaries are determined by considering the experimental resolution and migration effects. The bin edges are chosen so that the purity and stability of each bin is $\geq$50%. The bin edges for the $\rho$ variable correspond to about 1100, 750, 485, and 340 GeV for $m_{\text{t}\bar{\text{t}}+\text{jet}}$. The purity (stability) is defined as the number of signal events that are generated and reconstructed in the same bin, divided by the total number of signal events generated (reconstructed) in that bin. The unfolding problem is determined to be well conditioned, and therefore no regularization is required. To check for a possible bias of the fit, tests were performed where the true cross section was varied by a factor of two up and down for each parton-level bin, and the fit was repeated for each toy distribution. The fit was found to be unbiased.

### 6.1 Event categorization

The sensitivity of the cross section measurement to the different signal processes is enhanced by splitting the reconstructed events into multiple categories based on the jet ($N_{\text{jet}} = 1$, $N_{\text{jet}} = 2$, and $N_{\text{jet}} \geq 3$) and b jet multiplicities ($N_{\text{b jet}} = 1$ and $N_{\text{b jet}} \geq 2$) and the $\rho_{\text{reco}}$ bin. The different event types are labeled as "mjnb" for events with m jets and n b jets. Events with fewer than three reconstructed jets, corresponding mainly to background $\text{t}\bar{\text{t}}$+0 jet and Z+jets production, are also included in the fit. This maximizes the acceptance of the events reconstructed in the visible phase space and helps to constrain the background. Final-state distributions for each category are chosen that maximize the signal sensitivity. The relative signal response $R_{\text{NN}}$ of the NN classifier, defined as: $R_{\text{NN}} = s(\text{t}\bar{\text{t}}\text{+jet})/[s(\text{t}\bar{\text{t}}\text{+jet}) + s(\text{t}\bar{\text{t}}\text{+0 jet})]$, is used as the observable for event categories with more than two reconstructed jets. To increase the fit sensitivity to $m_{\text{t}}^{\text{MC}}$, the minimum invariant mass $m_{\ell\text{b}}^{\text{min}}$ among the lepton and b jet combinations is used as the observable for events with two jets, where both are b tagged. In the remaining categories, the $p_{\text{T}}$ of the lowest-$p_{\text{T}}$ jet is fitted. The three dileptonic channels are kept separate in the fit and are treated as independent categories to disentangle the effects of systematic uncertainties in the different lepton flavors. An overview of the event categories and the chosen distributions are given in table 1. Good agreement between the distributions from data and simulation is found.

In the binning of each observable, the statistical uncertainty in the nominal and systematic uncertainty templates is considered to reduce its impact on the extracted values of $r_k$, $w_j$, and $\vec{\lambda}$ after the fit to data. In particular, the kinematic distributions listed in table 1 are reduced to the total event yield if the number of simulated events is insufficient



JHEP07(2023)077

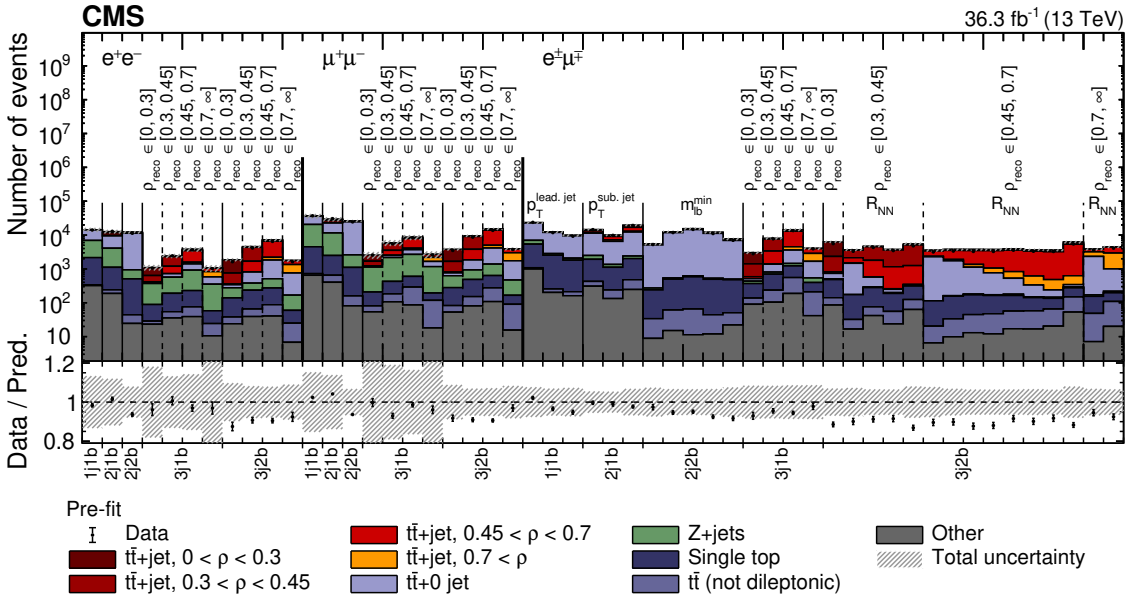


**Figure 6**. The distributions from data (points) and simulated signal and background (colored histograms) used in the maximum likelihood fits before the fit to the data. The distributions are shown for each dilepton type and each event category, where the x-axis label "mjnb" refers to events with m jets and n b jets. The vertical bars on the points show the statistical uncertainty in the data. The hatched band represents the total uncertainty in the sum of the simulated signal and background predictions. The lower panel gives the ratio of the data to the sum of the simulated predictions.

to model the kinematic distributions properly. As a criterion, the statistical uncertainty in the number of simulated events is not allowed to exceed 0.5% per bin. The final input distributions to the fit are displayed in figure 6, where the data are compared to the simulated signal and background distributions before the fit.

## 7 Systematic uncertainties

Contributions to the systematic uncertainties from various sources are modeled as nuisance parameters in the fit, as described in section 6. For each variation, dedicated templates are obtained describing the effect on each background source or signal contribution.

### 7.1 Experimental uncertainties

Most of the experimental systematic uncertainties are estimated by varying the scale factors (SFs) used to correct any differences between the data and simulation. The following experimental uncertainties are considered:

- The integrated luminosity used to normalize the simulated samples has a relative uncertainty of 1.2% [100].
- The uncertainty in the amount of pileup is estimated by varying the total inelastic pp cross section by its measurement uncertainty of 4.6% [77] in the simulation.



JHEP07(2023)077

- To correct for differences in the trigger efficiencies between data and simulation, dedicated SFs are derived in $p_T$ and $\eta$ bins of the leading and subleading leptons. These SFs are typically close to unity and are varied within their uncertainties, which are composed of statistical and systematic components are smaller than 3%.

- Electron and muon identification and isolation efficiencies are measured in bins of the lepton $p_T$ and $\eta$ [47, 48]. Corresponding uncertainties in the SFs are typically on the order of 2–5% for electrons, and 0.5–1.5% for muons. They are varied within their uncertainties in the simulation to estimate the corresponding systematic uncertainty.

- Uncertainties due to correcting the electron and muon energy scales and resolutions are assessed separately by varying them within their uncertainties in the simulation. The typical uncertainty in the energy resolution is on the order of 0.5% and 5% for electrons and muons, respectively [47, 48]. The energy variations are propagated to $\vec{p}_T^{\,\text{miss}}$.

- Several uncertainties affecting the correction of the jet energy scale (JES) are split into a set of 23 individual contributions [42]. They are varied as a function of the jet $p_T$ and $\eta$, and the effect is propagated to $\vec{p}_T^{\,\text{miss}}$. The total uncertainty in the JES ranges from 1.0–3.5% depending on the jet kinematic variables [42].

- An additional uncertainty in $\vec{p}_T^{\,\text{miss}}$ is derived by varying the energies of reconstructed particles not clustered into jets. Its effect on the resolution is on the order of 5–30% [101].

- The effect from the jet energy resolution (JER) is estimated by varying the SFs for the jet four-momenta within their uncertainty on the order of 2–8%, depending on the $\eta$ region [42].

- Uncertainties in the correction of the simulation coming from the application of the pileup jet identification are estimated by varying the efficiency and mistagging rate within their uncertainties [45, 102]. They range between 5–30%, depending on the jet $\eta$ and $p_T$.

- During the 2016 data taking, a gradual shift in the timing of the inputs to the ECAL L1 trigger in the region $|\eta| > 2.0$ caused a specific trigger inefficiency. For events containing an electron (jet) with $p_T$ larger than ≈50 (100) GeV, in the region $2.5 < |\eta| < 3.0$ the efficiency loss is ≈10–20%, depending on $p_T$, $\eta$, and the data-taking period [37]. A similar effect was present for L1-trigger muons because of the finite time resolution of the muon detectors, leading to an effect of 0.5–1.5% per muon [103]. Dedicated SFs are derived for correcting the simulation for this effect known as "prefiring" and are varied within their uncertainties.

- To correct for different b tagging efficiencies and mistagging rates of light-quark and gluon jets in the data and simulation, SFs are derived using simulated QCD multijet events and are applied as a function of the jet $p_T$ [80]. To estimate the impact of that



JHEP07(2023)077

systematic uncertainty, the SFs are varied within their estimated uncertainties, which are split into individual subsources. For light- and heavy-quark jets the uncertainty ranges from 5-10 and 1-5%, respectively.

### 7.2 Theoretical uncertainties

Additional systematic uncertainties arise from assumptions on the model parameters of the nominal POWHEG+PYTHIA8 simulation. Their effect is estimated by appropriate variations in the simulated samples. The following theoretical uncertainties are considered:

- To estimate the effect of missing higher-order corrections in the NLO simulation, the $\mu_R$ and $\mu_F$ scales are varied by a factor of two up and down in the POWHEG calculation with respect to their nominal values. Combined variations of $\mu_R$ and $\mu_F$ are not considered.

- Uncertainties in the modeling of the parton shower are assessed by varying individually the corresponding scales for the initial- (ISR) and final-state radiation (FSR) by a factor of two up and down with respect to their nominal values.

- The PDF uncertainty is estimated by using the 100 eigenvector variations of the NNPDF3.1 PDF set [52, 53], each treated as an individual nuisance parameter in the fit. Additionally, the value of $\alpha_S(m_Z)$, where $m_Z$ is the Z boson mass, is varied within its uncertainty in this PDF set.

- The dependence on the matching between the ME and PS generators is estimated by varying the $h_{damp}$ parameter in the POWHEG simulation within the tuning uncertainties [55] in dedicated simulated samples.

- The modeling dependence on the CP5 UE tune is evaluated by varying the tune parameters within their uncertainties [55], for which dedicated samples are generated.

- In the PYTHIA8 setup used for the nominal simulation, certain assumptions are made on the modeling of color reconnection (CR). While early-resonance decays (ERD) are turned off in the nominal setting, a dedicated sample with ERD enabled is generated, and the difference is treated as a systematic uncertainty. Moreover, alternative CR models are considered, including a gluon-move scheme [104] and a QCD-inspired scheme [105].

- Uncertainties originating from the limited knowledge of the b hadron fragmentation function are estimated by varying the parameters of the Bowler–Lund function within their uncertainties [106]. Alternatively, the Peterson fragmentation function [107] is used.

- The limited precision on the semileptonic branching fractions of b hadrons is estimated by varying them within their uncertainties, as estimated in ref. [4].



JHEP07(2023)077

- Differential measurements of the $\mathrm{t\bar{t}}$ cross section at $\sqrt{s} = 13\,\mathrm{TeV}$ have demonstrated that the $p_{\mathrm{T}}$ distribution of the top quark is softer than predicted by the POWHEG simulation [82–85, 108]. An additional uncertainty, which is estimated by reweighting the simulation to the measured top quark $p_{\mathrm{T}}$ in refs. [109, 110], is considered.

Besides the PDF and $h_{\mathrm{damp}}$ variations, all the above-mentioned uncertainties are also assessed for tW production and are considered correlated, if applicable. In the case of Z+jets production, $\mu_{\mathrm{R}}$ and $\mu_{\mathrm{F}}$ variations are also considered. The theoretical uncertainties in the extrapolation to the full phase space are estimated by evaluating their impact on the signal acceptance following the strategy of refs. [22, 32]. The extrapolation uncertainty is determined after varying each nuisance parameter individually according to their uncertainties before the fit and by recomputing the cross section and evaluating the difference with respect to the nominal result. The extrapolation uncertainty is determined as described in the following. Each relevant nuisance parameter $j$ is set to values corresponding to one standard deviation up and down while all others are fixed to the values after the fit. The resulting changes in the acceptance are recorded. The corresponding variations of the cross section values $\sigma^{k}_{\mathrm{t\bar{t}+jet}}$ with respect to the nominal values are considered as the additional relative extrapolation uncertainty.

### 7.3 Additional uncertainties

Additional uncertainties arise from the normalizations of the background processes, the finite number of events in the MC simulation, and the corresponding effects on the templates from these sources.

The uncertainties in the normalizations for single top quark production and smaller background contributions, such as diboson and W+jets production, are taken to be 30% and modeled with a log-normal prior pdf, following the prescriptions from previous analyses [22, 29, 85]. For the Z+jets background, separate uncertainties are used for each b jet category in order to remove the dependence of the fit result on the prediction of the b jet multiplicity distribution from the Z+jets simulation. Similarly, the Z+jets background is assigned an additional uncertainty of 5, 10, 30, and 50% for events with exactly 0, 1, 2, and 3 or more jets, respectively. The first three uncertainties are estimated by performing scale variations in the W+jets predictions with NLO precision, whereas the last one is assigned conservatively [22]. For the $\mathrm{t\bar{t}}$+0 jet background, no prior pdf is used since the normalization is left free in the fit in order to help constrain it with the background-dominated categories.

The statistical uncertainty due to the finite size of the MC event samples is evaluated via bin-by-bin nuisance parameters with the Barlow–Beeston "light" method [99, 111]. In addition, the impact of the finite statistical precision on the predictions of the MC samples with dedicated systematic variations is cross-checked using toy experiments, following the approach described in ref. [32], and was found to be negligible.

## 8 Results and extraction of the top quark mass

Figure 7 compares the resulting data distributions after the fit to the MC signal and background predictions. The measured absolute differential cross section $\mathrm{d}\sigma_{\mathrm{t\bar{t}+jet}}/\mathrm{d}\rho$ is



JHEP07(2023)077

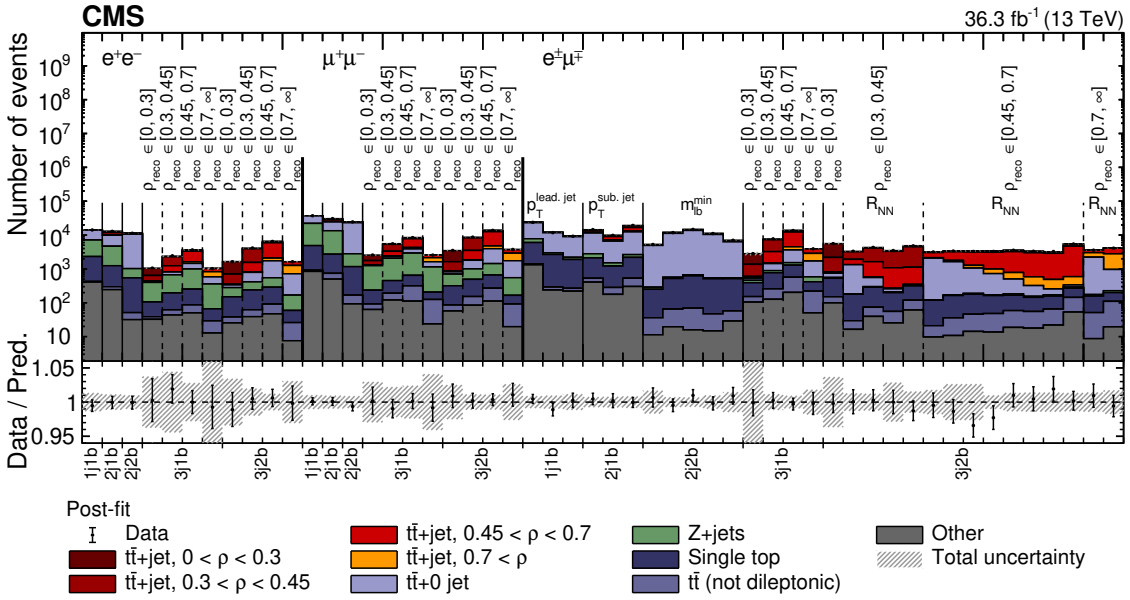


**Figure 7**. The distributions from data (points) and simulated signal and background (colored histograms) used in the maximum likelihood fits after the fit to the data. The distributions are shown for each dilepton type and each event category, where the x-axis label "$mjn$b" refers to events with $m$ jets and $n$ b jets. The vertical bars on the points show the statistical uncertainty in the data. The hatched band represents the total uncertainty in the sum of the simulated signal and background predictions. The lower panel gives the ratio of the data to the sum of the simulated predictions.

shown in figure 8 (left) and compared to the NLO QCD predictions. The latter are obtained using the $\mathrm{t\bar{t}}$+jet process implemented in POWHEG-BOX [112], with the ABMP16NLO [113] PDF set, and assuming $m_{\mathrm{t}}^{\mathrm{pole}}$ values of 169.5, 172.5, and 175.5 GeV. The same kinematic requirements on the additional jet as defined in section 3.1 are used, while the simulation is not interfaced to any parton shower. It is worth mentioning that in the ABMP analysis, the PDFs and $\alpha_{\mathrm{S}}(m_{\mathrm{Z}})$ are obtained simultaneously at the same perturbative order in QCD. Additionally, the CT18NLO PDF set [114] is considered.

The QCD scale in the theoretical prediction is dynamically set to $H_{\mathrm{T}}^{B}/2$, as suggested in ref. [115] and discussed in ref. [116], where $H_{\mathrm{T}}^{B}$ is defined as the scalar sum of the top quark and antiquark transverse masses and the $p_{\mathrm{T}}$ of the additional jet. The values and the uncertainty in the normalized differential cross section are derived from the fit results for the absolute cross section by taking into account the covariance matrix as obtained in the fit to data. The normalized differential cross section is determined by dividing the value of the absolute differential cross section for each bin by the sum of the values of all the bins. Uncertainties are symmetrized prior to the normalization as provided by HESSE [95]. The results are shown in figure 8 (right) in comparison with the theoretical predictions. While the absolute cross section shows a stronger dependence on $\alpha_{\mathrm{S}}$, this dependence is small for the normalized cross section [116]. All the sources and values of the systematic uncertainties in the differential cross section result are given in table 2.



JHEP07(2023)077

| Uncertainty Source | $\Delta\sigma^{1}_{t\bar{t}+\text{jet}}$ [%] | $\Delta\sigma^{2}_{t\bar{t}+\text{jet}}$ [%] | $\Delta\sigma^{3}_{t\bar{t}+\text{jet}}$ [%] | $\Delta\sigma^{4}_{t\bar{t}+\text{jet}}$ [%] |
|---|---|---|---|---|
| Experimental | | | | |
| Muon identification | 1.8 | 1.5 | 1.5 | 1.4 |
| Muon energy scale and resolution | 0.7 | 0.2 | 0.3 | 0.5 |
| Electron identification | 2.0 | 1.7 | 1.7 | 2.1 |
| Electron energy scale and resolution | 0.9 | 1.0 | 0.9 | 1.5 |
| Jet energy scale | 2.6 | 2.0 | 2.2 | 3.6 |
| Jet energy resolution | 0.6 | 0.5 | 0.5 | 0.4 |
| Jet identification | 1.1 | 0.8 | 0.8 | 1.3 |
| $p_{\text{T}}^{\text{miss}}$ | 0.2 | 0.3 | 0.4 | 0.8 |
| b jet identification | 1.0 | 0.7 | 0.6 | 1.2 |
| Trigger efficiency | 1.8 | 1.2 | 1.1 | 1.8 |
| Total | 4.0 | 3.1 | 3.1 | 4.7 |
| Background normalization | | | | |
| $t\bar{t}$+0 jet | 2.2 | 2.0 | 1.7 | 0.7 |
| Z+jets | 2.4 | 1.9 | 1.7 | 2.6 |
| Single top quark | 0.9 | 0.8 | 0.7 | 0.1 |
| Total | 3.1 | 2.5 | 2.4 | 2.7 |
| Modeling | | | | |
| Z+jets ME scale | 0.7 | 0.4 | 0.2 | 0.3 |
| Single top quark ME/FSR/ISR scales | 1.2 | 0.6 | 0.4 | 0.1 |
| $t\bar{t}$ PDF | 0.1 | 0.1 | 0.1 | 0.6 |
| $t\bar{t}$ ME scale | 1.0 | 0.5 | 0.6 | 0.4 |
| $t\bar{t}$ ISR scale | 1.2 | 0.8 | 0.6 | 1.6 |
| $t\bar{t}$ FSR scale | 1.3 | 0.8 | 0.6 | 1.7 |
| $t\bar{t}$ top quark $p_{\text{T}}$ | 2.0 | 1.3 | 0.1 | 1.2 |
| b fragmentation | 0.9 | 0.7 | 0.8 | 0.8 |
| Color reconnection | 0.5 | 0.6 | 0.2 | 0.7 |
| $t\bar{t}$ matching scale | 0.6 | 0.5 | 0.6 | $\leq$0.1 |
| Underlying-event tune | 0.2 | 0.5 | 0.2 | 0.5 |
| Total | 3.2 | 1.9 | 1.8 | 3.1 |
| Integrated luminosity | 1.2 | 1.4 | 1.3 | 1.2 |
| $m_{\text{t}}^{\text{MC}}$ | 1.7 | 1.0 | 0.4 | 2.3 |
| Finite size of simulated samples | 2.0 | 1.4 | 1.3 | 2.2 |
| Total systematic | 5.0 | 3.4 | 3.2 | 5.6 |
| Statistical | 1.6 | 1.0 | 0.8 | 2.4 |
| Total | 5.2 | 3.6 | 3.3 | 6.1 |

**Table 2**. The relative uncertainties $\Delta\sigma^{k}_{t\bar{t}+\text{jet}}$ in the parton-level cross section values $\sigma^{k}_{t\bar{t}+\text{jet}}$ and their sources in each bin $k$ of the $\rho$ distribution. The statistical uncertainty is evaluated by keeping all nuisance parameters fixed to their values after the fit to data. The breakdown of the uncertainty is obtained by repeating the fit after fixing the nuisance parameters related to the components under consideration to their fitted values. The partial uncertainty is then estimated by subtracting the uncertainty obtained with this procedure from the total uncertainty. The quadratic sum of the contributions is different from the total uncertainty because of correlations between the nuisance parameters.

JHEP07(2023)077

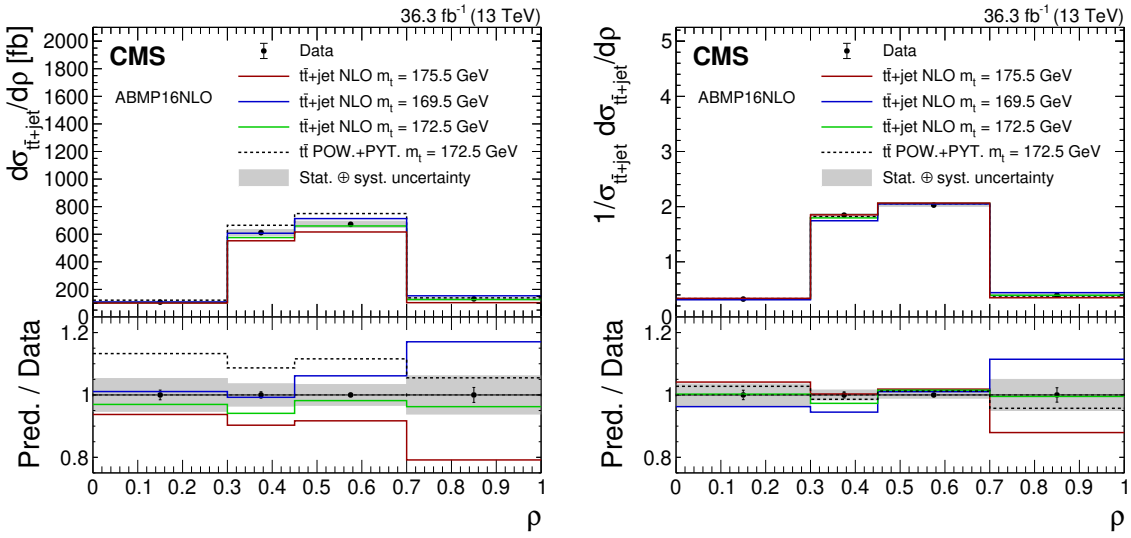


**Figure 8**. The absolute (left) and normalized (right) $\mathrm{t\bar{t}}$+jet differential cross section as a function of $\rho$ for the data (points) and theoretical predictions described in the text using the AMBP16NLO PDF set from the NLO MC with three different $m_\mathrm{t}$ values and from the POWHEG (POW) + PYTHIA8 (PYT) calculations (lines). The vertical bars on the points show the statistical uncertainty in the data and the shaded region represents the total uncertainty in the measurement. The lower panels give the ratio of the predictions to the data.

The fitted parameter values, expected and observed constraints, and impacts on the signal strengths $r_k$ for the 30 most important nuisance parameters after the fit to data are shown in figure 9. For each parameter, the difference between the best fit ($\hat{\theta}$) and input value ($\theta_0$) is given relative to the input uncertainty $\Delta\theta$, while the constraint is defined as the uncertainty after the fit relative to the input uncertainty. For the nuisance parameters associated with the $\mathrm{t\bar{t}}$+0 jet normalization and $m_\mathrm{t}^\mathrm{MC}$, the values of the nuisance parameters after the fit are given in the figure instead of plotting $(\hat{\theta} - \theta_0)/\Delta\theta$ because no prior pdf is assigned. The values of the nuisance parameters after the fit are compatible with the corresponding values before the fit within their prior uncertainties, reflecting the good agreement between data and simulation before the fit. Some differences between $\hat{\theta}$ and $\theta_0$ for nuisance parameters describing the background normalization for the single top quark and Z+jets processes are larger. This is expected because of the limitations in the MC simulations used to model these backgrounds in the signal phase space region, which often corresponds to the tails of the background processes. The nuisance parameter associated with the modeling of the top quark $p_\mathrm{T}$ spectra also has a larger value after the fit. This is because of the different spectra observed in data and simulation, as discussed in section 4.

The observed constraints and impacts agree with the expectations derived from fitting pseudo-data obtained from the nominal simulation. Strong constraints are determined on the normalizations of the background Z+jets and single top quark processes, which are explained by their large number of events in the background-dominated categories that helps to constrain the large normalization uncertainty. The nuisance parameter associated



JHEP07(2023)077

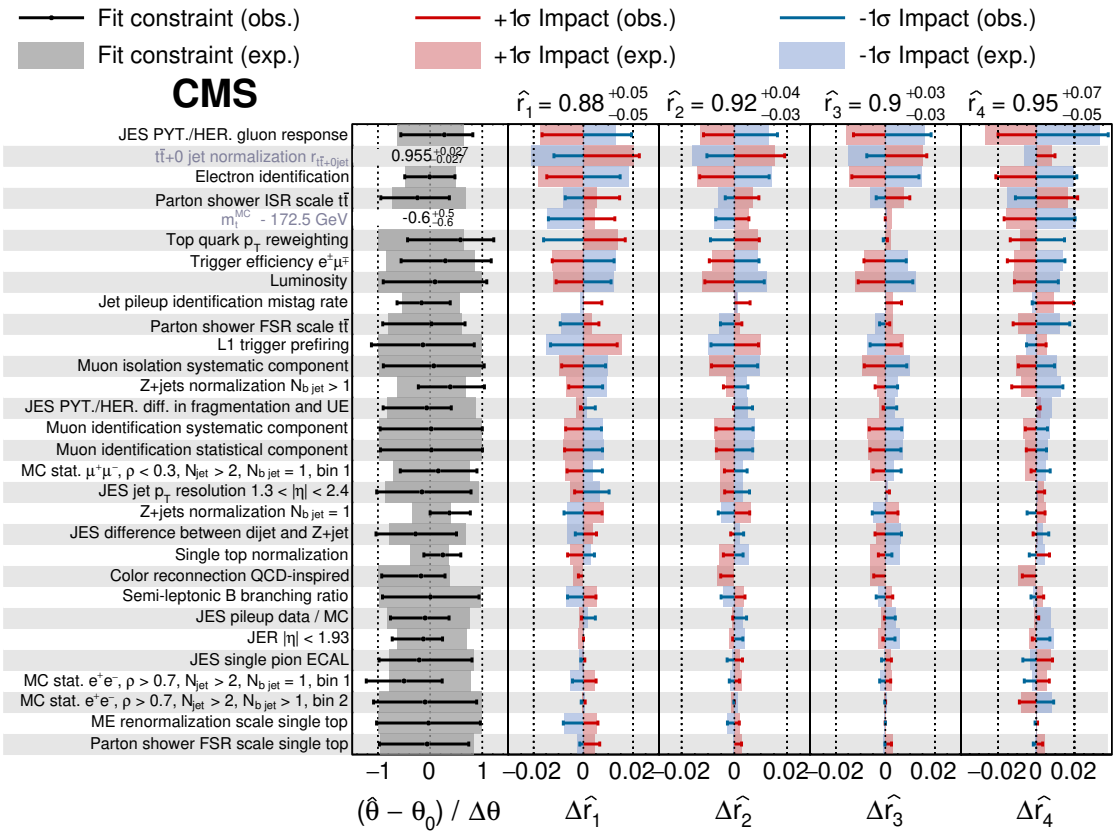


**Figure 9**. The fitted nuisance-parameter values and their impacts $\Delta\hat{r}_k$ on the signal strengths $\hat{r}_k$ from the fit to the data, ordered by their relative summed impact. Only the 30 highest ranked parameters are shown. The resulting fitted values of $\hat{r}_k$ and their total uncertainties are also given. The nuisance-parameter values ($\hat{\theta}$, black lines) are shown in comparison to their input values $\theta_0$ before the fit and relative to their uncertainty $\Delta\theta$. The impact $\Delta\hat{r}_k$ for each nuisance parameter is the difference between the nominal best fit value of $r_k$ and the best fit value when only that nuisance parameter is set to its best fit value $\hat{\theta}$ while all others are left free. The red and blue lines correspond to the variation in $\Delta\hat{r}_k$ when the nuisance parameter is varied up and down by its fitted uncertainty ($\Delta\theta$), respectively. The corresponding gray, red, and blue regions show the expected values from fits to pseudo-data. For the nuisance parameters associated with the $t\bar{t}$+0 jet normalization and $m_t^{MC}$, the values after the fit to the data are given, because no prior pdf is assigned.

with the electron identification efficiency has a tight constraint from combining decay channels with different electron and muon multiplicities in the fit. This effect was seen in previous CMS measurements [22, 32].

The constraints on nuisance parameters associated with the jet energy corrections, JER, and jet identification demonstrate the power of the fit method, since the analysis phase space region and fitted kinematic distributions are sensitive to these effects. Also, because the analyzed phase space region is different from the one used to derive the corresponding calibrations described in section 7, deviations from the values before the fit and constraints are expected. In the fit, $m_t^{MC}$ is determined as $171.93 \pm 0.65$ GeV, where the uncertainty includes both the statistical and systematic components.



JHEP07(2023)077

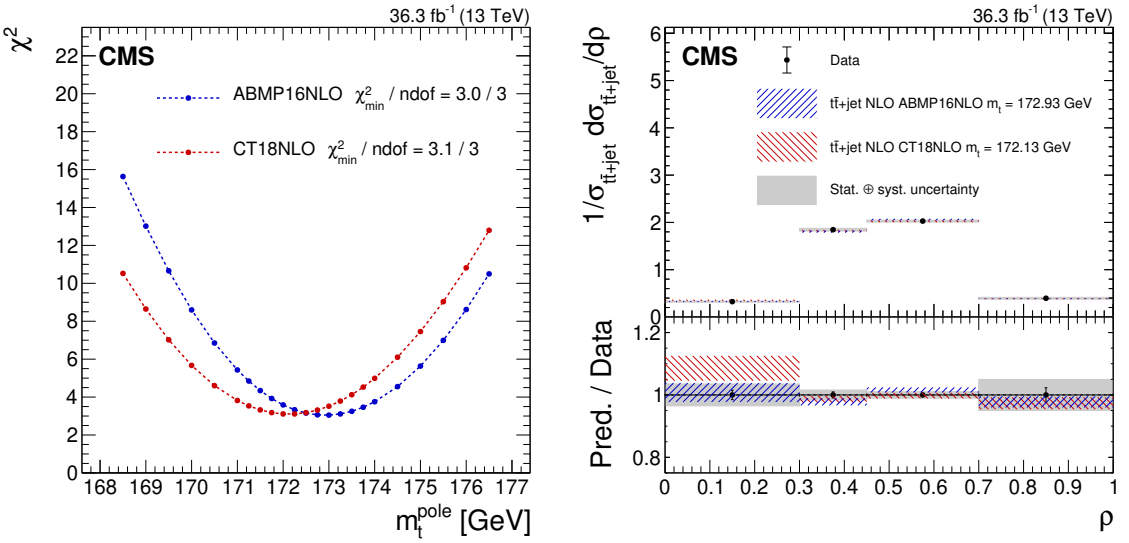


**Figure 10**. Left: The $\chi^2$ values versus $m_t^{pole}$ from the fit of the measured normalized $t\bar{t}$+jet differential cross sections to the theoretical predictions using the ABMP16NLO (blue points) and CT18NLO (red points) PDF sets. The minimum $\chi^2$ value and the number of degrees of freedom (ndof) are given for each fit. Right: The measured normalized $t\bar{t}$+jet differential cross section (points) as a function of $\rho$, compared to the predictions using the two PDF sets and the corresponding best fit values for $m_t^{pole}$ (hatched bands). The lower panel gives the ratio of the theoretical predictions to the measured values. For both panels, the vertical bars on the points show the statistical uncertainty in the data, the height of the hatched bands represent the theoretical uncertainties in the predictions, and the gray band gives the total uncertainty in the measured cross section.

The value of $m_t^{pole}$ is extracted from a $\chi^2$ fit of the theoretical predictions for the normalized differential cross section at NLO to the measurement. Since in a fit to a normalized distribution, the value of any bin is fully determined by the value of the others, one bin is removed from the $\chi^2$ fit. The result is independent of the choice of the removed bin. The covariance matrix used in the $\chi^2$ fit is derived by combining the one obtained in the likelihood fit, the extrapolation uncertainties in the measured cross section, and the PDF uncertainties in the theoretical predictions. The PDF uncertainties are evaluated in each bin and included in the total covariance matrix. For CT18NLO, the uncertainties evaluated at 90% confidence level (CL), are rescaled to the 68% CL for consistency with the ABMP16NLO PDF set and symmetrized by taking the maximum of the up and down variation. The extrapolation uncertainties for all relevant theoretical uncertainties, as described in section 7, are symmetrized by taking the average of the positive and negative impacts and are included in the calculation of the $\chi^2$. The resulting $\chi^2$ curves are shown in figure 10 (left). The best fit value for $m_t^{pole}$ is extracted at the $\chi^2$ minimum and the experimental uncertainty is obtained using the tolerance criterion of $\Delta\chi^2 = 1$.

To estimate the scale variation uncertainty, the fit is repeated using the theoretical predictions, with $\mu_R$ and $\mu_F$ varied independently by factors of 0.5 and 2, avoiding cases where $\mu_F/\mu_R = 4$ or 1/4. The total scale uncertainty is estimated by taking the maximum



JHEP07(2023)077

difference in the results to the nominal one. The resulting value of

$$m_{\mathrm{t}}^{\mathrm{pole}} = 172.93 \pm 1.26\,(\mathrm{fit})\,^{+0.51}_{-0.43}\,(\mathrm{scale})\,\mathrm{GeV}$$

is obtained using the ABMP16NLO PDF set. The first uncertainty corresponds to the total statistical and systematic uncertainties from the fit including the PDF and extrapolation uncertainties, and the second uncertainty comes from the variation in the $\mu_{\mathrm{R}}$ and $\mu_{\mathrm{F}}$ scales. Using the CT18NLO PDF set instead, the measured value is

$$m_{\mathrm{t}}^{\mathrm{pole}} = 172.13 \pm 1.34\,(\mathrm{fit})\,^{+0.50}_{-0.40}\,(\mathrm{scale})\,\mathrm{GeV}.$$

The total uncertainty in $m_{\mathrm{t}}^{\mathrm{pole}}$ corresponds to 1.36 (1.43) GeV for the ABMP16NLO (CT18NLO) PDF set. Comparisons between the unfolded data and theoretical predictions for the determined values of $m_{\mathrm{t}}^{\mathrm{pole}}$ with both PDF sets are given in figure 10 (right), showing good agreement between the fitted prediction and the measured cross section for both PDF sets. The impact of the individual PDF uncertainties is estimated by replacing the central values of the measured cross section with the ones obtained from the theoretical prediction, assuming a top quark mass of 172.5 GeV. Two fits are performed: one using the full covariance matrix, and the other with a covariance matrix that excludes the effect of the PDF uncertainties. The difference in quadrature of the two results represents an approximate estimate of the impact of the PDF uncertainties. This procedure yields a total impact of 0.35 (0.27) GeV for the CT18NLO (ABMP16NLO) PDF set.

The obtained results are in good agreement with previous measurements of $m_{\mathrm{t}}^{\mathrm{pole}}$ using $\mathrm{t\bar{t}}$+jet events [35] at a center-of-mass energy of 8 TeV by ATLAS and the triple-differential cross sections for $\mathrm{t\bar{t}}$ production at a center-of-mass energy of 13 TeV by CMS [29]. Compared to the ATLAS result, a lower sensitivity to $m_{\mathrm{t}}^{\mathrm{pole}}$ is expected in this analysis due to the higher center-of-mass energy. Furthermore, in this analysis the systematic uncertainty due to the PDFs is fully taken into account, which leads to an increase in the total uncertainty in $m_{\mathrm{t}}^{\mathrm{pole}}$.

## 9 Summary

Measurements are presented of the normalized differential cross section of top quark-antiquark pair ($\mathrm{t\bar{t}}$) production in association with at least one additional jet as a function of the inverse of the invariant mass of the $\mathrm{t\bar{t}}$+jet system $\rho = 2m_0/m_{\mathrm{t\bar{t}+jet}}$, with the scaling constant $m_0 = 170$ GeV. Proton-proton collision data collected by the CMS experiment at the CERN LHC at a center-of-mass energy of 13 TeV are used, corresponding to an integrated luminosity of 36.3 $\mathrm{fb}^{-1}$. Events in the dilepton decay channel are considered, and a novel multivariate analysis technique is applied to maximize the sensitivity to the signal process. The differential cross section is measured at the parton level using a maximum likelihood fit to final-state observables, where all systematic uncertainties are profiled. The value of the top quark pole mass $m_{\mathrm{t}}^{\mathrm{pole}}$ is extracted by comparing the measured $\mathrm{t\bar{t}}$+jet normalized differential cross section as a function of $\rho$ to theoretical predictions at next-to-leading order in quantum chromodynamics, obtained with two sets of parton distribution



JHEP07(2023)077

functions. The $m_{\mathrm{t}}^{\mathrm{pole}}$ values is determined to be $172.93 \pm 1.36\,\mathrm{GeV}$ and $172.13 \pm 1.43\,\mathrm{GeV}$ using the ABMP16NLO and CT18NLO parton distribution functions, respectively. Here, the uncertainties shown include the total statistical and systematic uncertainties including extrapolation uncertainties, and the theoretical uncertainties from the parton distribution functions and the matrix-element scales. The results are in good agreement with previous measurements.

## Acknowledgments

We congratulate our colleagues in the CERN accelerator departments for the excellent performance of the LHC and thank the technical and administrative staffs at CERN and at other CMS institutes for their contributions to the success of the CMS effort. In addition, we gratefully acknowledge the computing centers and personnel of the Worldwide LHC Computing Grid and other centers for delivering so effectively the computing infrastructure essential to our analyses. Finally, we acknowledge the enduring support for the construction and operation of the LHC, the CMS detector, and the supporting computing infrastructure provided by the following funding agencies: BMBWF and FWF (Austria); FNRS and FWO (Belgium); CNPq, CAPES, FAPERJ, FAPERGS, and FAPESP (Brazil); MES and BNSF (Bulgaria); CERN; CAS, MoST, and NSFC (China); MINCIENCIAS (Colombia); MSES and CSF (Croatia); RIF (Cyprus); SENESCYT (Ecuador); MoER, ERC PUT and ERDF (Estonia); Academy of Finland, MEC, and HIP (Finland); CEA and CNRS/IN2P3 (France); BMBF, DFG, and HGF (Germany); GSRI (Greece); NKFIH (Hungary); DAE and DST (India); IPM (Iran); SFI (Ireland); INFN (Italy); MSIP and NRF (Republic of Korea); MES (Latvia); LAS (Lithuania); MOE and UM (Malaysia); BUAP, CINVESTAV, CONACYT, LNS, SEP, and UASLP-FAI (Mexico); MOS (Montenegro); MBIE (New Zealand); PAEC (Pakistan); MES and NSC (Poland); FCT (Portugal); MESTD (Serbia); MCIN/AEI and PCTI (Spain); MOSTR (Sri Lanka); Swiss Funding Agencies (Switzerland); MST (Taipei); MHESI and NSTDA (Thailand); TUBITAK and TENMAK (Turkey); NASU (Ukraine); STFC (United Kingdom); DOE and NSF (USA).

Individuals have received support from the Marie-Curie programme and the European Research Council and Horizon 2020 Grant, contract Nos. 675440, 724704, 752730, 758316, 765710, 824093, 884104, and COST Action CA16108 (European Union); the Leventis Foundation; the Alfred P. Sloan Foundation; the Alexander von Humboldt Foundation; the Belgian Federal Science Policy Office; the Fonds pour la Formation à la Recherche dans l'Industrie et dans l'Agriculture (FRIA-Belgium); the Agentschap voor Innovatie door Wetenschap en Technologie (IWT-Belgium); the F.R.S.-FNRS and FWO (Belgium) under the "Excellence of Science — EOS" — be.h project n. 30820817; the Beijing Municipal Science & Technology Commission, No. Z191100007219010; the Ministry of Education, Youth and Sports (MEYS) of the Czech Republic; the Hellenic Foundation for Research and Innovation (HFRI), Project Number 2288 (Greece); the Deutsche Forschungsgemeinschaft (DFG), under Germany's Excellence Strategy — EXC 2121 "Quantum Universe" – 390833306, and under project number 400140256 — GRK2497; the Hungarian Academy of Sciences, the New National Excellence Program — ÚNKP, the NKFIH re-



JHEP07(2023)077

search grants K 124845, K 124850, K 128713, K 128786, K 129058, K 131991, K 133046, K 138136, K 143460, K 143477, 2020-2.2.1-ED-2021-00181, and TKP2021-NKTA-64 (Hungary); the Council of Science and Industrial Research, India; the Latvian Council of Science; the Ministry of Education and Science, project no. 2022/WK/14, and the National Science Center, contracts Opus 2021/41/B/ST2/01369 and 2021/43/B/ST2/01552 (Poland); the Fundação para a Ciência e a Tecnologia, grant CEECIND/01334/2018 (Portugal); the National Priorities Research Program by Qatar National Research Fund; MCIN/AEI/10.13039/501100011033, ERDF "a way of making Europe", and the Programa Estatal de Fomento de la Investigación Científica y Técnica de Excelencia María de Maeztu, grant MDM-2017-0765 and Programa Severo Ochoa del Principado de Asturias (Spain); the Chulalongkorn Academic into Its 2nd Century Project Advancement Project, and the National Science, Research and Innovation Fund via the Program Management Unit for Human Resources & Institutional Development, Research and Innovation, grant B05F650021 (Thailand); the Kavli Foundation; the Nvidia Corporation; the SuperMicro Corporation; the Welch Foundation, contract C-1845; and the Weston Havens Foundation (USA).



## References

[1] Gfitter Group collaboration, *The global electroweak fit at NNLO and prospects for the LHC and ILC*, *Eur. Phys. J. C* **74** (2014) 3046 [arXiv:1407.3792] [INSPIRE].

[2] J. de Blas et al., *Electroweak precision observables and Higgs-boson signal strengths in the Standard Model and beyond: present and future*, *JHEP* **12** (2016) 135 [arXiv:1608.01509] [INSPIRE].

[3] S. Alekhin, J. Blümlein, S. Moch and R. Placakyte, *Parton distribution functions, $\alpha_s$, and heavy-quark masses for LHC Run II*, *Phys. Rev. D* **96** (2017) 014011 [arXiv:1701.05838] [INSPIRE].

[4] Particle Data Group collaboration, *Review of Particle Physics*, *PTEP* **2020** (2020) 083C01 [INSPIRE].

[5] G. Degrassi et al., *Higgs mass and vacuum stability in the Standard Model at NNLO*, *JHEP* **08** (2012) 098 [arXiv:1205.6497] [INSPIRE].

[6] S. Alekhin, A. Djouadi and S. Moch, *The top quark and Higgs boson masses and the stability of the electroweak vacuum*, *Phys. Lett. B* **716** (2012) 214 [arXiv:1207.0980] [INSPIRE].

[7] ATLAS collaboration, *Measurement of the top quark mass in the $t\bar{t} \to$ dilepton channel from $\sqrt{s} = 8$ TeV ATLAS data*, *Phys. Lett. B* **761** (2016) 350 [arXiv:1606.02179] [INSPIRE].

[8] ATLAS collaboration, *Top-quark mass measurement in the all-hadronic $t\bar{t}$ decay channel at $\sqrt{s} = 8$ TeV with the ATLAS detector*, *JHEP* **09** (2017) 118 [arXiv:1702.07546] [INSPIRE].

[9] ATLAS collaboration, *Measurement of the top quark mass in the $t\bar{t} \to$ lepton+jets channel from $\sqrt{s} = 8$ TeV ATLAS data and combination with previous results*, *Eur. Phys. J. C* **79** (2019) 290 [arXiv:1810.01772] [INSPIRE].



JHEP07(2023)077

[10] CMS collaboration, *Measurement of the top quark mass using proton-proton data at* $\sqrt{(s)} = 7$ *and* 8 *TeV*, *Phys. Rev. D* **93** (2016) 072004 [arXiv:1509.04044] [INSPIRE].

[11] CMS collaboration, *Measurement of the top quark mass in the dileptonic* $t\bar{t}$ *decay channel using the mass observables* $M_{b\ell}$, $M_{T2}$, *and* $M_{b\ell\nu}$ *in pp collisions at* $\sqrt{s} = 8$ *TeV*, *Phys. Rev. D* **96** (2017) 032002 [arXiv:1704.06142] [INSPIRE].

[12] CMS collaboration, *Measurement of the top quark mass with lepton+jets final states using pp collisions at* $\sqrt{s} = 13$ *TeV*, *Eur. Phys. J. C* **78** (2018) 891 [*Erratum ibid.* **82** (2022) 323] [arXiv:1805.01428] [INSPIRE].

[13] CMS collaboration, *Measurement of the top quark mass in the all-jets final state at* $\sqrt{s} = 13$ *TeV and combination with the lepton+jets channel*, *Eur. Phys. J. C* **79** (2019) 313 [arXiv:1812.10534] [INSPIRE].

[14] CMS collaboration, *Measurement of the top quark mass using events with a single reconstructed top quark in pp collisions at* $\sqrt{s} = 13$ *TeV*, *JHEP* **12** (2021) 161 [arXiv:2108.10407] [INSPIRE].

[15] S. Ferrario Ravasio, T. Ježo, P. Nason and C. Oleari, *A theoretical study of top-mass measurements at the LHC using NLO+PS generators of increasing accuracy*, *Eur. Phys. J. C* **78** (2018) 458 [*Addendum ibid.* **79** (2019) 859] [arXiv:1906.09166] [INSPIRE].

[16] M. Butenschoen et al., *Top quark mass calibration for Monte Carlo event generators*, *Phys. Rev. Lett.* **117** (2016) 232001 [arXiv:1608.01318] [INSPIRE].

[17] ATLAS, CDF, CMS, and D0 collaborations, *First combination of Tevatron and LHC measurements of the top-quark mass*, arXiv:1403.4427 [INSPIRE].

[18] S. Moch et al., *High precision fundamental constants at the TeV scale*, arXiv:1405.4781 [INSPIRE].

[19] A. Juste et al., *Determination of the top quark mass circa 2013: methods, subtleties, perspectives*, *Eur. Phys. J. C* **74** (2014) 3119 [arXiv:1310.0799] [INSPIRE].

[20] A.H. Hoang, *What is the top quark mass?*, *Ann. Rev. Nucl. Part. Sci.* **70** (2020) 225 [arXiv:2004.12915] [INSPIRE].

[21] A.H. Hoang, *The Top Mass: Interpretation and Theoretical Uncertainties*, in the proceedings of the *7th International Workshop on Top Quark Physics*, Cannes, France, September 28–October 3 (2014) [arXiv:1412.3649] [INSPIRE].

[22] CMS collaboration, *Measurement of the* $t\bar{t}$ *production cross section, the top quark mass, and the strong coupling constant using dilepton events in pp collisions at* $\sqrt{s} = 13$ *TeV*, *Eur. Phys. J. C* **79** (2019) 368 [arXiv:1812.10505] [INSPIRE].

[23] ATLAS collaboration, *Measurement of the* $t\bar{t}$ *production cross-section using* $e\mu$ *events with b-tagged jets in pp collisions at* $\sqrt{s} = 7$ *and* 8 *TeV with the ATLAS detector*, *Eur. Phys. J. C* **74** (2014) 3109 [*Addendum ibid.* **76** (2016) 642] [arXiv:1406.5375] [INSPIRE].

[24] CMS collaboration, *Measurement of the* $t\bar{t}$ *production cross section in the* $e\mu$ *channel in proton-proton collisions at* $\sqrt{s} = 7$ *and* 8 *TeV*, *JHEP* **08** (2016) 029 [arXiv:1603.02303] [INSPIRE].

[25] CMS collaboration, *Measurement of the* $t\bar{t}$ *production cross section using events with one lepton and at least one jet in pp collisions at* $\sqrt{s} = 13$ *TeV*, *JHEP* **09** (2017) 051 [arXiv:1701.06228] [INSPIRE].



JHEP07(2023)077

[26] ATLAS collaboration, *Determination of the top-quark pole mass using $t\bar{t}$ + 1-jet events collected with the ATLAS experiment in 7 TeV pp collisions*, *JHEP* **10** (2015) 121 [arXiv:1507.01769] [INSPIRE].

[27] D0 collaboration, *Measurement of the inclusive $t\bar{t}$ production cross section in $p\bar{p}$ collisions at $\sqrt{s} = 1.96$ TeV and determination of the top quark pole mass*, *Phys. Rev. D* **94** (2016) 092004 [arXiv:1605.06168] [INSPIRE].

[28] ATLAS collaboration, *Measurement of lepton differential distributions and the top quark mass in $t\bar{t}$ production in pp collisions at $\sqrt{s} = 8$ TeV with the ATLAS detector*, *Eur. Phys. J. C* **77** (2017) 804 [arXiv:1709.09407] [INSPIRE].

[29] CMS collaboration, *Measurement of $t\bar{t}$ normalised multi-differential cross sections in pp collisions at $\sqrt{s} = 13$ TeV, and simultaneous determination of the strong coupling strength, top quark pole mass, and parton distribution functions*, *Eur. Phys. J. C* **80** (2020) 658 [arXiv:1904.05237] [INSPIRE].

[30] U. Langenfeld, S. Moch and P. Uwer, *Measuring the running top-quark mass*, *Phys. Rev. D* **80** (2009) 054009 [arXiv:0906.5273] [INSPIRE].

[31] J. Fuster et al., *Extracting the top-quark running mass using $t\bar{t}$+ 1-jet events produced at the Large Hadron Collider*, *Eur. Phys. J. C* **77** (2017) 794 [arXiv:1704.00540] [INSPIRE].

[32] CMS collaboration, *Running of the top quark mass from proton-proton collisions at $\sqrt{s} = 13$ TeV*, *Phys. Lett. B* **803** (2020) 135263 [arXiv:1909.09193] [INSPIRE].

[33] S. Alioli et al., *A new observable to measure the top-quark mass at hadron colliders*, *Eur. Phys. J. C* **73** (2013) 2438 [arXiv:1303.6415] [INSPIRE].

[34] G. Bevilacqua et al., *Top quark mass studies with $t\bar{t}j$ at the LHC*, *JHEP* **03** (2018) 169 [arXiv:1710.07515] [INSPIRE].

[35] ATLAS collaboration, *Measurement of the top-quark mass in $t\bar{t} + 1$-jet events collected with the ATLAS detector in pp collisions at $\sqrt{s} = 8$ TeV*, *JHEP* **11** (2019) 150 [arXiv:1905.02302] [INSPIRE].

[36] CMS collaboration, *Measurement of the top quark pole mass using $t\bar{t}$+jet events in the dilepton final state in proton-proton collisions at $\sqrt{s} = 13$ TeV*, https://www.hepdata.net/record/ins2106483 [DOI:10.17182/HEPDATA.127990].

[37] CMS collaboration, *Performance of the CMS Level-1 trigger in proton-proton collisions at $\sqrt{s} = 13$ TeV*, 2020 *JINST* **15** P10017 [arXiv:2006.10165] [INSPIRE].

[38] CMS collaboration, *The CMS trigger system*, 2017 *JINST* **12** P01020 [arXiv:1609.02366] [INSPIRE].

[39] CMS collaboration, *The CMS Experiment at the CERN LHC*, 2008 *JINST* **3** S08004 [INSPIRE].

[40] D. Contardo et al., *Technical Proposal for the Phase-II Upgrade of the CMS Detector*, CERN-LHCC-2015-010 (2015) [DOI:10.17181/CERN.VU8I.D59J].

[41] CMS collaboration, *Particle-flow reconstruction and global event description with the CMS detector*, 2017 *JINST* **12** P10003 [arXiv:1706.04965] [INSPIRE].

[42] CMS collaboration, *Jet energy scale and resolution in the CMS experiment in pp collisions at 8 TeV*, 2017 *JINST* **12** P02014 [arXiv:1607.03663] [INSPIRE].

JHEP07(2023)077

[43] CMS collaboration, *Performance of missing transverse momentum reconstruction in proton-proton collisions at $\sqrt{s} = 13$ TeV using the CMS detector*, 2019 *JINST* **14** P07004 [arXiv:1903.06078] [INSPIRE].

[44] D. Bertolini, P. Harris, M. Low and N. Tran, *Pileup per particle identification*, *JHEP* **10** (2014) 059 [arXiv:1407.6013] [INSPIRE].

[45] CMS collaboration, *Pileup mitigation at CMS in* 13 *TeV data*, 2020 *JINST* **15** P09018 [arXiv:2003.00503] [INSPIRE].

[46] CMS collaboration, *ECAL 2016 refined calibration and Run2 summary plots*, CMS-DP-2020-021 (2020).

[47] CMS collaboration, *Electron and photon reconstruction and identification with the CMS experiment at the CERN LHC*, 2021 *JINST* **16** P05014 [arXiv:2012.06888] [INSPIRE].

[48] CMS collaboration, *Performance of the CMS muon detector and muon reconstruction with proton-proton collisions at $\sqrt{s} = 13$ TeV*, 2018 *JINST* **13** P06015 [arXiv:1804.04528] [INSPIRE].

[49] S. Frixione, P. Nason and C. Oleari, *Matching NLO QCD computations with Parton Shower simulations: the POWHEG method*, *JHEP* **11** (2007) 070 [arXiv:0709.2092] [INSPIRE].

[50] S. Frixione, P. Nason and G. Ridolfi, *A positive-weight next-to-leading-order Monte Carlo for heavy flavour hadroproduction*, *JHEP* **09** (2007) 126 [arXiv:0707.3088] [INSPIRE].

[51] S. Alioli, P. Nason, C. Oleari and E. Re, *A general framework for implementing NLO calculations in shower Monte Carlo programs: the POWHEG BOX*, *JHEP* **06** (2010) 043 [arXiv:1002.2581] [INSPIRE].

[52] NNPDF collaboration, *Unbiased global determination of parton distributions and their uncertainties at NNLO and at LO*, *Nucl. Phys. B* **855** (2012) 153 [arXiv:1107.2652] [INSPIRE].

[53] NNPDF collaboration, *Parton distributions from high-precision collider data*, *Eur. Phys. J. C* **77** (2017) 663 [arXiv:1706.00428] [INSPIRE].

[54] T. Sjöstrand et al., *An introduction to PYTHIA 8.2*, *Comput. Phys. Commun.* **191** (2015) 159 [arXiv:1410.3012] [INSPIRE].

[55] CMS collaboration, *Extraction and validation of a new set of CMS PYTHIA8 tunes from underlying-event measurements*, *Eur. Phys. J. C* **80** (2020) 4 [arXiv:1903.12179] [INSPIRE].

[56] J. Alwall et al., *The automated computation of tree-level and next-to-leading order differential cross sections, and their matching to parton shower simulations*, *JHEP* **07** (2014) 079 [arXiv:1405.0301] [INSPIRE].

[57] R. Frederix and S. Frixione, *Merging meets matching in MC@NLO*, *JHEP* **12** (2012) 061 [arXiv:1209.6215] [INSPIRE].

[58] P. Artoisenet, R. Frederix, O. Mattelaer and R. Rietkerk, *Automatic spin-entangled decays of heavy resonances in Monte Carlo simulations*, *JHEP* **03** (2013) 015 [arXiv:1212.3460] [INSPIRE].

[59] E. Re, *Single-top Wt-channel production matched with parton showers using the POWHEG method*, *Eur. Phys. J. C* **71** (2011) 1547 [arXiv:1009.2450] [INSPIRE].



JHEP07(2023)077

[60] S. Alioli, P. Nason, C. Oleari and E. Re, *NLO single-top production matched with shower in POWHEG: s- and t-channel contributions*, *JHEP* **09** (2009) 111 [*Erratum ibid.* **02** (2010) 011] [arXiv:0907.4076] [INSPIRE].

[61] CMS collaboration, *Investigations of the impact of the parton shower tuning in Pythia 8 in the modelling of $t\bar{t}$ at $\sqrt{s} = 8$ and 13 TeV*, CMS-PAS-TOP-16-021, CERN, Geneva (2016).

[62] CMS collaboration, *Event generator tunes obtained from underlying event and multiparton scattering measurements*, *Eur. Phys. J. C* **76** (2016) 155 [arXiv:1512.00815] [INSPIRE].

[63] P. Skands, S. Carrazza and J. Rojo, *Tuning PYTHIA 8.1: the Monash 2013 Tune*, *Eur. Phys. J. C* **74** (2014) 3024 [arXiv:1404.5630] [INSPIRE].

[64] M.L. Mangano, M. Moretti, F. Piccinini and M. Treccani, *Matching matrix elements and shower evolution for top-quark production in hadronic collisions*, *JHEP* **01** (2007) 013 [hep-ph/0611129] [INSPIRE].

[65] S. Mrenna and P. Richardson, *Matching matrix elements and parton showers with HERWIG and PYTHIA*, *JHEP* **05** (2004) 040 [hep-ph/0312274] [INSPIRE].

[66] M. Czakon and A. Mitov, *Top++: a program for the calculation of the top-pair cross-section at hadron colliders*, *Comput. Phys. Commun.* **185** (2014) 2930 [arXiv:1112.5675] [INSPIRE].

[67] M. Cacciari et al., *Top-pair production at hadron colliders with next-to-next-to-leading logarithmic soft-gluon resummation*, *Phys. Lett. B* **710** (2012) 612 [arXiv:1111.5869] [INSPIRE].

[68] P. Bärnreuther, M. Czakon and A. Mitov, *Percent level precision physics at the Tevatron: first genuine NNLO QCD corrections to $q\bar{q} \to t\bar{t} + X$*, *Phys. Rev. Lett.* **109** (2012) 132001 [arXiv:1204.5201] [INSPIRE].

[69] M. Czakon and A. Mitov, *NNLO corrections to top-pair production at hadron colliders: the all-fermionic scattering channels*, *JHEP* **12** (2012) 054 [arXiv:1207.0236] [INSPIRE].

[70] M. Czakon and A. Mitov, *NNLO corrections to top pair production at hadron colliders: the quark-gluon reaction*, *JHEP* **01** (2013) 080 [arXiv:1210.6832] [INSPIRE].

[71] M. Beneke, P. Falgari, S. Klein and C. Schwinn, *Hadronic top-quark pair production with NNLL threshold resummation*, *Nucl. Phys. B* **855** (2012) 695 [arXiv:1109.1536] [INSPIRE].

[72] M. Czakon, P. Fiedler and A. Mitov, *Total top-quark pair-production cross section at hadron colliders through $O(\alpha_S^4)$*, *Phys. Rev. Lett.* **110** (2013) 252004 [arXiv:1303.6254] [INSPIRE].

[73] N. Kidonakis, *Two-loop soft anomalous dimensions for single top quark associated production with a $W^-$ or $H^-$*, *Phys. Rev. D* **82** (2010) 054018 [arXiv:1005.4451] [INSPIRE].

[74] J.M. Campbell, R.K. Ellis and C. Williams, *Vector boson pair production at the LHC*, *JHEP* **07** (2011) 018 [arXiv:1105.0020] [INSPIRE].

[75] Y. Li and F. Petriello, *Combining QCD and electroweak corrections to dilepton production in FEWZ*, *Phys. Rev. D* **86** (2012) 094034 [arXiv:1208.5967] [INSPIRE].

[76] GEANT4 collaboration, *GEANT4 — a simulation toolkit*, *Nucl. Instrum. Meth. A* **506** (2003) 250 [INSPIRE].

[77] ATLAS collaboration, *Measurement of the inelastic proton-proton cross section at $\sqrt{s} = 13$*



JHEP07(2023)077

*TeV with the ATLAS detector at the LHC*, *Phys. Rev. Lett.* **117** (2016) 182002 [arXiv:1606.02625] [INSPIRE].

[78] M. Cacciari, G.P. Salam and G. Soyez, *The anti-$k_t$ jet clustering algorithm*, *JHEP* **04** (2008) 063 [arXiv:0802.1189] [INSPIRE].

[79] M. Cacciari, G.P. Salam and G. Soyez, *FastJet user manual*, *Eur. Phys. J. C* **72** (2012) 1896 [arXiv:1111.6097] [INSPIRE].

[80] CMS collaboration, *Identification of heavy-flavour jets with the CMS detector in pp collisions at* 13 *TeV*, 2018 *JINST* **13** P05011 [arXiv:1712.07158] [INSPIRE].

[81] CMS collaboration, *A deep neural network for simultaneous estimation of b jet energy and resolution*, *Comput. Softw. Big Sci.* **4** (2020) 10 [arXiv:1912.06046] [INSPIRE].

[82] CMS collaboration, *Measurement of the differential cross section for top quark pair production in pp collisions at $\sqrt{s} = 8$ TeV*, *Eur. Phys. J. C* **75** (2015) 542 [arXiv:1505.04480] [INSPIRE].

[83] CMS collaboration, *Measurement of double-differential cross sections for top quark pair production in pp collisions at $\sqrt{s} = 8$ TeV and impact on parton distribution functions*, *Eur. Phys. J. C* **77** (2017) 459 [arXiv:1703.01630] [INSPIRE].

[84] CMS collaboration, *Measurement of normalized differential $t\bar{t}$ cross sections in the dilepton channel from pp collisions at $\sqrt{s} = 13$ TeV*, *JHEP* **04** (2018) 060 [arXiv:1708.07638] [INSPIRE].

[85] CMS collaboration, *Measurements of $t\bar{t}$ differential cross sections in proton-proton collisions at $\sqrt{s} = 13$ TeV using events containing two leptons*, *JHEP* **02** (2019) 149 [arXiv:1811.06625] [INSPIRE].

[86] L. Sonnenschein, *Analytical solution of $t\bar{t}$ dilepton equations*, *Phys. Rev. D* **73** (2006) 054015 [*Erratum ibid.* **78** (2008) 079902] [hep-ph/0603011] [INSPIRE].

[87] M. Abadi et al., *TensorFlow: large-scale machine learning on heterogeneous distributed systems*, arXiv:1603.04467 [INSPIRE].

[88] F. Chollet et al., *Keras*, https://keras.io (2015)

[89] J. Snoek, H. Larochelle and R.P. Adams, *Practical Bayesian optimization of machine learning algorithms*, arXiv:1206.2944.

[90] E. Brochu, V.M. Cora and N. de Freitas, *A tutorial on bayesian optimization of expensive cost functions, with application to active user modeling and hierarchical reinforcement learning*, arXiv:1012.2599.

[91] F. Nogueira, *Bayesian optimization: open source constrained global optimization tool for Python*, https://github.com/fmfn/BayesianOptimization.

[92] R.D. Cousins, *Generalization of chisquare goodness-of-fit test for binned data using saturated models, with application to histograms* (2013).

[93] Y. Ganin and V. Lempitsky, *Unsupervised domain adaptation by backpropagation*, arXiv:1409.7495.

[94] J. Kieseler, K. Lipka and S.-O. Moch, *Calibration of the top-quark Monte Carlo mass*, *Phys. Rev. Lett.* **116** (2016) 162001 [arXiv:1511.00841] [INSPIRE].

[95] F. James and M. Roos, *Minuit: a system for function minimization and analysis of the parameter errors and correlations*, *Comput. Phys. Commun.* **10** (1975) 343 [INSPIRE].



JHEP07(2023)077

[96] ATLAS et al. collaborations, *Procedure for the LHC Higgs boson search combination in Summer 2011*, CMS-NOTE-2011-005, CERN, Geneva (2011).

[97] CMS collaboration, *Precise determination of the mass of the Higgs boson and tests of compatibility of its couplings with the standard model predictions using proton collisions at 7 and 8 TeV*, *Eur. Phys. J. C* **75** (2015) 212 [arXiv:1412.8662] [INSPIRE].

[98] ATLAS and CMS collaborations, *Measurements of the Higgs boson production and decay rates and constraints on its couplings from a combined ATLAS and CMS analysis of the LHC pp collision data at* $\sqrt{s} = 7$ *and* 8 *TeV*, *JHEP* **08** (2016) 045 [arXiv:1606.02266] [INSPIRE].

[99] J.S. Conway, *Incorporating Nuisance Parameters in Likelihoods for Multisource Spectra*, in the proceedings of the *PHYSTAT 2011*, Geneva, Switzerland, January 17–20 (2011), p. 115–120 [DOI:10.5170/CERN-2011-006.115] [arXiv:1103.0354] [INSPIRE].

[100] CMS collaboration, *Precision luminosity measurement in proton-proton collisions at* $\sqrt{s} = 13$ *TeV in 2015 and 2016 at CMS*, *Eur. Phys. J. C* **81** (2021) 800 [arXiv:2104.01927] [INSPIRE].

[101] CMS collaboration, *Performance of missing energy reconstruction in* 13 *TeV pp collision data using the CMS detector*, CMS-PAS-JME-16-004, CERN, Geneva (2016).

[102] CMS collaboration, *Performance of the pile up jet identification in CMS for Run 2*, CMS-DP-2020-020 (2020).

[103] CMS collaboration, *Performance of the CMS muon trigger system in proton-proton collisions at* $\sqrt{s} = 13$ *TeV*, 2021 *JINST* **16** P07001 [arXiv:2102.04790] [INSPIRE].

[104] S. Argyropoulos and T. Sjöstrand, *Effects of color reconnection on* $t\bar{t}$ *final states at the LHC*, *JHEP* **11** (2014) 043 [arXiv:1407.6653] [INSPIRE].

[105] J.R. Christiansen and P.Z. Skands, *String formation beyond leading colour*, *JHEP* **08** (2015) 003 [arXiv:1505.01681] [INSPIRE].

[106] M.G. Bowler, $e^+e^-$ *production of heavy quarks in the string model*, *Z. Phys. C* **11** (1981) 169 [INSPIRE].

[107] C. Peterson, D. Schlatter, I. Schmitt and P.M. Zerwas, *Scaling violations in inclusive* $e^+e^-$ *annihilation spectra*, *Phys. Rev. D* **27** (1983) 105 [INSPIRE].

[108] CMS collaboration, *Measurement of the* $t\bar{t}$ *production cross section in the all-jets final state in pp collisions at* $\sqrt{s} = 8$ *TeV*, *Eur. Phys. J. C* **76** (2016) 128 [arXiv:1509.06076] [INSPIRE].

[109] CMS collaboration, *Measurement of differential cross sections for top quark pair production using the lepton+jets final state in proton-proton collisions at 13 TeV*, *Phys. Rev. D* **95** (2017) 092001 [arXiv:1610.04191] [INSPIRE].

[110] CMS collaboration, *Measurement of the differential cross section for* $t\bar{t}$ *production in the dilepton final state at* $\sqrt{s} = 13$ *TeV*, CMS-PAS-TOP-16-011, CERN, Geneva (2016).

[111] R.J. Barlow and C. Beeston, *Fitting using finite Monte Carlo samples*, *Comput. Phys. Commun.* **77** (1993) 219 [INSPIRE].

[112] S. Alioli, S.-O. Moch and P. Uwer, *Hadronic top-quark pair-production with one jet and parton showering*, *JHEP* **01** (2012) 137 [arXiv:1110.5251] [INSPIRE].



JHEP07(2023)077

[113] S. Alekhin, J. Blümlein and S. Moch, *NLO PDFs from the ABMP16 fit*, *Eur. Phys. J. C* **78** (2018) 477 [arXiv:1803.07537] [INSPIRE].

[114] T.-J. Hou et al., *Progress in the CTEQ-TEA NNLO global QCD analysis*, arXiv:1908.11394 [INSPIRE].

[115] G. Bevilacqua, H.B. Hartanto, M. Kraus and M. Worek, *Off-shell top quarks with one jet at the LHC: a comprehensive analysis at NLO QCD*, *JHEP* **11** (2016) 098 [arXiv:1609.01659] [INSPIRE].

[116] S. Alioli et al., *Phenomenology of $t\bar{t}j$ + X production at the LHC*, *JHEP* **05** (2022) 146 [arXiv:2202.07975] [INSPIRE].

JHEP07(2023)077

## The CMS collaboration


### Yerevan Physics Institute, Yerevan, Armenia

A. Tumasyan[1]

### Institut für Hochenergiephysik, Vienna, Austria

W. Adam, J.W. Andrejkovic, T. Bergauer, S. Chatterjee, K. Damanakis, M. Dragicevic, A. Escalante Del Valle, P.S. Hussain, M. Jeitler[2], N. Krammer, L. Lechner, D. Liko, I. Mikulec, P. Paulitsch, F.M. Pitters, J. Schieck[2], R. Schöfbeck, D. Schwarz, S. Templ, W. Waltenberger, C.-E. Wulz[2]

### Universiteit Antwerpen, Antwerpen, Belgium

M.R. Darwish[3], T. Janssen, T. Kello[4], H. Rejeb Sfar, P. Van Mechelen

### Vrije Universiteit Brussel, Brussel, Belgium

E.S. Bols, J. D'Hondt, A. De Moor, M. Delcourt, H. El Faham, S. Lowette, S. Moortgat, A. Morton, D. Müller, A.R. Sahasransu, S. Tavernier, W. Van Doninck, D. Vannerom

### Université Libre de Bruxelles, Bruxelles, Belgium

B. Clerbaux, G. De Lentdecker, L. Favart, D. Hohov, J. Jaramillo, K. Lee, M. Mahdavikhorrami, I. Makarenko, A. Malara, S. Paredes, L. Pétré, N. Postiau, E. Starling, L. Thomas, M. Vanden Bemden, C. Vander Velde, P. Vanlaer

### Ghent University, Ghent, Belgium

D. Dobur, J. Knolle, L. Lambrecht, G. Mestdach, M. Niedziela, C. Rendón, C. Roskas, A. Samalan, K. Skovpen, M. Tytgat, N. Van Den Bossche, B. Vermassen, L. Wezenbeek

### Université Catholique de Louvain, Louvain-la-Neuve, Belgium

A. Benecke, G. Bruno, F. Bury, C. Caputo, P. David, C. Delaere, I.S. Donertas, A. Giammanco, K. Jaffel, Sa. Jain, V. Lemaitre, K. Mondal, J. Prisciandaro, A. Taliercio, T.T. Tran, P. Vischia, S. Wertz

### Centro Brasileiro de Pesquisas Fisicas, Rio de Janeiro, Brazil

G.A. Alves, E. Coelho, C. Hensel, A. Moraes, P. Rebello Teles

### Universidade do Estado do Rio de Janeiro, Rio de Janeiro, Brazil

W.L. Aldá Júnior, M. Alves Gallo Pereira, M. Barroso Ferreira Filho, H. Brandao Malbouisson, W. Carvalho, J. Chinellato[5], E.M. Da Costa, G.G. Da Silveira[6], D. De Jesus Damiao, V. Dos Santos Sousa, S. Fonseca De Souza, J. Martins[7], C. Mora Herrera, K. Mota Amarilo, L. Mundim, H. Nogima, A. Santoro, S.M. Silva Do Amaral, A. Sznajder, M. Thiel, F. Torres Da Silva De Araujo[8], A. Vilela Pereira


JHEP07(2023)077

**Universidade Estadual Paulista, Universidade Federal do ABC, São Paulo, Brazil**

C.A. Bernardes[6], L. Calligaris, T.R. Fernandez Perez Tomei, E.M. Gregores, P.G. Mercadante, S.F. Novaes, Sandra S. Padula

**Institute for Nuclear Research and Nuclear Energy, Bulgarian Academy of Sciences, Sofia, Bulgaria**

A. Aleksandrov, G. Antchev, R. Hadjiiska, P. Iaydjiev, M. Misheva, M. Rodozov, M. Shopova, G. Sultanov

**University of Sofia, Sofia, Bulgaria**

A. Dimitrov, T. Ivanov, L. Litov, B. Pavlov, P. Petkov, A. Petrov, E. Shumka

**Beihang University, Beijing, China**

T. Cheng, T. Javaid[9], M. Mittal, L. Yuan

**Department of Physics, Tsinghua University, Beijing, China**

M. Ahmad, G. Bauer[10], Z. Hu, S. Lezki, K. Yi[10,11]

**Institute of High Energy Physics, Beijing, China**

G.M. Chen[9], H.S. Chen[9], M. Chen[9], F. Iemmi, C.H. Jiang, A. Kapoor, H. Liao, Z.-A. Liu[12], V. Milosevic, F. Monti, R. Sharma, J. Tao, J. Thomas-Wilsker, J. Wang, H. Zhang, J. Zhao

**State Key Laboratory of Nuclear Physics and Technology, Peking University, Beijing, China**

A. Agapitos, Y. An, Y. Ban, C. Chen, A. Levin, C. Li, Q. Li, X. Lyu, Y. Mao, S.J. Qian, X. Sun, D. Wang, J. Xiao, H. Yang

**Sun Yat-Sen University, Guangzhou, China**

M. Lu, Z. You

**Institute of Modern Physics and Key Laboratory of Nuclear Physics and Ion-beam Application (MOE) - Fudan University, Shanghai, China**

X. Gao[4], D. Leggat, H. Okawa, Y. Zhang

**Zhejiang University, Hangzhou, Zhejiang, China**

Z. Lin, C. Lu, M. Xiao

**Universidad de Los Andes, Bogota, Colombia**

C. Avila, D.A. Barbosa Trujillo, A. Cabrera, C. Florez, J. Fraga

**Universidad de Antioquia, Medellin, Colombia**

J. Mejia Guisao, F. Ramirez, M. Rodriguez, J.D. Ruiz Alvarez

**University of Split, Faculty of Electrical Engineering, Mechanical Engineering and Naval Architecture, Split, Croatia**

D. Giljanovic, N. Godinovic, D. Lelas, I. Puljak

JHEP07(2023)077

**University of Split, Faculty of Science, Split, Croatia**
Z. Antunovic, M. Kovac, T. Sculac

**Institute Rudjer Boskovic, Zagreb, Croatia**
V. Brigljevic, B.K. Chitroda, D. Ferencek, D. Majumder, M. Roguljic, A. Starodumov[13], T. Susa

**University of Cyprus, Nicosia, Cyprus**
A. Attikis, K. Christoforou, G. Kole, M. Kolosova, S. Konstantinou, J. Mousa, C. Nicolaou, F. Ptochos, P.A. Razis, H. Rykaczewski, H. Saka

**Charles University, Prague, Czech Republic**
M. Finger[13], M. Finger Jr.[13], A. Kveton

**Escuela Politecnica Nacional, Quito, Ecuador**
E. Ayala

**Universidad San Francisco de Quito, Quito, Ecuador**
E. Carrera Jarrin

**Academy of Scientific Research and Technology of the Arab Republic of Egypt, Egyptian Network of High Energy Physics, Cairo, Egypt**
H. Abdalla[14], Y. Assran[15,16]

**Center for High Energy Physics (CHEP-FU), Fayoum University, El-Fayoum, Egypt**
M.A. Mahmoud, Y. Mohammed

**National Institute of Chemical Physics and Biophysics, Tallinn, Estonia**
S. Bhowmik, R.K. Dewanjee, K. Ehataht, M. Kadastik, T. Lange, S. Nandan, C. Nielsen, J. Pata, M. Raidal, L. Tani, C. Veelken

**Department of Physics, University of Helsinki, Helsinki, Finland**
P. Eerola, H. Kirschenmann, K. Osterberg, M. Voutilainen

**Helsinki Institute of Physics, Helsinki, Finland**
S. Bharthuar, E. Brücken, F. Garcia, J. Havukainen, M.S. Kim, R. Kinnunen, T. Lampén, K. Lassila-Perini, S. Lehti, T. Lindén, M. Lotti, L. Martikainen, M. Myllymäki, J. Ott, M.m. Rantanen, H. Siikonen, E. Tuominen, J. Tuominiemi

**Lappeenranta-Lahti University of Technology, Lappeenranta, Finland**
P. Luukka, H. Petrow, T. Tuuva

**IRFU, CEA, Université Paris-Saclay, Gif-sur-Yvette, France**
C. Amendola, M. Besancon, F. Couderc, M. Dejardin, D. Denegri, J.L. Faure, F. Ferri, S. Ganjour, P. Gras, G. Hamel de Monchenault, P. Jarry, V. Lohezic, J. Malcles, J. Rander, A. Rosowsky, M.Ö. Sahin, A. Savoy-Navarro[17], P. Simkina, M. Titov

JHEP07(2023)077

**Laboratoire Leprince-Ringuet, CNRS/IN2P3, Ecole Polytechnique, Institut Polytechnique de Paris, Palaiseau, France**

C. Baldenegro Barrera, F. Beaudette, A. Buchot Perraguin, P. Busson, A. Cappati, C. Charlot, F. Damas, O. Davignon, B. Diab, G. Falmagne, B.A. Fontana Santos Alves, S. Ghosh, R. Granier de Cassagnac, A. Hakimi, B. Harikrishnan, G. Liu, J. Motta, M. Nguyen, C. Ochando, L. Portales, J. Rembser, R. Salerno, U. Sarkar, J.B. Sauvan, Y. Sirois, A. Tarabini, E. Vernazza, A. Zabi, A. Zghiche

**Université de Strasbourg, CNRS, IPHC UMR 7178, Strasbourg, France**

J.-L. Agram[18], J. Andrea, D. Apparu, D. Bloch, G. Bourgatte, J.-M. Brom, E.C. Chabert, C. Collard, D. Darej, U. Goerlach, C. Grimault, A.-C. Le Bihan, P. Van Hove

**Institut de Physique des 2 Infinis de Lyon (IP2I ), Villeurbanne, France**

S. Beauceron, C. Bernet, B. Blancon, G. Boudoul, A. Carle, N. Chanon, J. Choi, D. Contardo, P. Depasse, C. Dozen[19], H. El Mamouni, J. Fay, S. Gascon, M. Gouzevitch, G. Grenier, B. Ille, I.B. Laktineh, M. Lethuillier, L. Mirabito, S. Perries, L. Torterotot, M. Vander Donckt, P. Verdier, S. Viret

**Georgian Technical University, Tbilisi, Georgia**

I. Lomidze, T. Toriashvili[20], Z. Tsamalaidze[13]

**RWTH Aachen University, I. Physikalisches Institut, Aachen, Germany**

V. Botta, L. Feld, K. Klein, M. Lipinski, D. Meuser, A. Pauls, N. Röwert, M. Teroerde

**RWTH Aachen University, III. Physikalisches Institut A, Aachen, Germany**

S. Diekmann, A. Dodonova, N. Eich, D. Eliseev, M. Erdmann, P. Fackeldey, D. Fasanella, B. Fischer, T. Hebbeker, K. Hoepfner, F. Ivone, M.y. Lee, L. Mastrolorenzo, M. Merschmeyer, A. Meyer, S. Mondal, S. Mukherjee, D. Noll, A. Novak, F. Nowotny, A. Pozdnyakov, Y. Rath, W. Redjeb, H. Reithler, A. Schmidt, S.C. Schuler, A. Sharma, L. Vigilante, S. Wiedenbeck, S. Zaleski

**RWTH Aachen University, III. Physikalisches Institut B, Aachen, Germany**

C. Dziwok, G. Flügge, W. Haj Ahmad[21], O. Hlushchenko, T. Kress, A. Nowack, O. Pooth, A. Stahl[22], T. Ziemons, A. Zotz

**Deutsches Elektronen-Synchrotron, Hamburg, Germany**

H. Aarup Petersen, M. Aldaya Martin, P. Asmuss, S. Baxter, M. Bayatmakou, O. Behnke, A. Bermúdez Martínez, S. Bhattacharya, A.A. Bin Anuar, F. Blekman[23], K. Borras[24], D. Brunner, A. Campbell, A. Cardini, C. Cheng, F. Colombina, S. Consuegra Rodríguez, G. Correia Silva, M. De Silva, L. Didukh, G. Eckerlin, D. Eckstein, L.I. Estevez Banos, O. Filatov, E. Gallo[23], A. Geiser, A. Giraldi, G. Greau, A. Grohsjean, V. Guglielmi, M. Guthoff, A. Jafari[25], N.Z. Jomhari,

JHEP07(2023)077

B. Kaech, A. Kasem[24], M. Kasemann, H. Kaveh, C. Kleinwort, R. Kogler, M. Komm, D. Krücker, W. Lange, D. Leyva Pernia, K. Lipka, W. Lohmann[26], R. Mankel, I.-A. Melzer-Pellmann, M. Mendizabal Morentin, J. Metwally, A.B. Meyer, G. Milella, S.O. Moch, M. Mormile, A. Mussgiller, A. Nürnberg, Y. Otarid, D. Pérez Adán, A. Raspereza, B. Ribeiro Lopes, J. Rübenach, A. Saggio, A. Saibel, M. Savitskyi, M. Scham[27,24], V. Scheurer, S. Schnake[24], P. Schütze, C. Schwanenberger[23], M. Shchedrolosiev, R.E. Sosa Ricardo, D. Stafford, N. Tonon[†], M. Van De Klundert, F. Vazzoler, A. Ventura Barroso, K. Voß, R. Walsh, D. Walter, Q. Wang, Y. Wen, K. Wichmann, L. Wiens[24], C. Wissing, S. Wuchterl, Y. Yang, A. Zimermmane Castro Santos

**University of Hamburg, Hamburg, Germany**

R. Aggleton, A. Albrecht, S. Albrecht, M. Antonello, S. Bein, L. Benato, M. Bonanomi, P. Connor, K. De Leo, M. Eich, K. El Morabit, F. Feindt, A. Fröhlich, C. Garbers, E. Garutti, M. Hajheidari, J. Haller, A. Hinzmann, H.R. Jabusch, G. Kasieczka, R. Klanner, W. Korcari, T. Kramer, V. Kutzner, J. Lange, A. Lobanov, C. Matthies, A. Mehta, L. Moureaux, M. Mrowietz, A. Nigamova, Y. Nissan, A. Paasch, K.J. Pena Rodriguez, M. Rieger, O. Rieger, P. Schleper, M. Schröder, J. Schwandt, H. Stadie, G. Steinbrück, A. Tews, M. Wolf

**Karlsruher Institut fuer Technologie, Karlsruhe, Germany**

J. Bechtel, S. Brommer, M. Burkart, E. Butz, R. Caspart, T. Chwalek, A. Dierlamm, A. Droll, N. Faltermann, M. Giffels, J.O. Gosewisch, A. Gottmann, F. Hartmann[22], M. Horzela, U. Husemann, P. Keicher, M. Klute, R. Koppenhöfer, S. Maier, S. Mitra, Th. Müller, M. Neukum, G. Quast, K. Rabbertz, J. Rauser, D. Savoiu, M. Schnepf, D. Seith, I. Shvetsov, H.J. Simonis, N. Trevisani, R. Ulrich, J. van der Linden, R.F. Von Cube, M. Wassmer, M. Weber, S. Wieland, R. Wolf, S. Wozniewski, S. Wunsch

**Institute of Nuclear and Particle Physics (INPP), NCSR Demokritos, Aghia Paraskevi, Greece**

G. Anagnostou, P. Assiouras, G. Daskalakis, A. Kyriakis, A. Stakia

**National and Kapodistrian University of Athens, Athens, Greece**

M. Diamantopoulou, D. Karasavvas, P. Kontaxakis, A. Manousakis-Katsikakis, A. Panagiotou, I. Papavergou, N. Saoulidou, K. Theofilatos, E. Tziaferi, K. Vellidis, E. Vourliotis, I. Zisopoulos

**National Technical University of Athens, Athens, Greece**

G. Bakas, T. Chatzistavrou, K. Kousouris, I. Papakrivopoulos, G. Tsipolitis, A. Zacharopoulou

**University of Ioánnina, Ioánnina, Greece**

K. Adamidis, I. Bestintzanos, I. Evangelou, C. Foudas, P. Gianneios, C. Kamtsikis, P. Katsoulis, P. Kokkas, P.G. Kosmoglou Kioseoglou, N. Manthos, I. Papadopoulos, J. Strologas

JHEP07(2023)077

**MTA-ELTE Lendület CMS Particle and Nuclear Physics Group, Eötvös Loránd University, Budapest, Hungary**

M. Csanád, K. Farkas, M.M.A. Gadallah[28], S. Lökös[29], P. Major, K. Mandal, G. Pásztor, A.J. Rádl[30], O. Surányi, G.I. Veres

**Wigner Research Centre for Physics, Budapest, Hungary**

M. Bartók[31], G. Bencze, C. Hajdu, D. Horvath[32,33], F. Sikler, V. Veszpremi

**Institute of Nuclear Research ATOMKI, Debrecen, Hungary**

N. Beni, S. Czellar, J. Karancsi[31], J. Molnar, Z. Szillasi, D. Teyssier

**Institute of Physics, University of Debrecen, Debrecen, Hungary**

P. Raics, B. Ujvari[34]

**Karoly Robert Campus, MATE Institute of Technology, Gyongyos, Hungary**

T. Csorgo[30], F. Nemes[30], T. Novak

**Panjab University, Chandigarh, India**

J. Babbar, S. Bansal, S.B. Beri, V. Bhatnagar, G. Chaudhary, S. Chauhan, N. Dhingra[35], R. Gupta, A. Kaur, A. Kaur, H. Kaur, M. Kaur, S. Kumar, P. Kumari, M. Meena, K. Sandeep, T. Sheokand, J.B. Singh[36], A. Singla, A. K. Virdi

**University of Delhi, Delhi, India**

A. Ahmed, A. Bhardwaj, B.C. Choudhary, M. Gola, S. Keshri, A. Kumar, M. Naimuddin, P. Priyanka, K. Ranjan, S. Saumya, A. Shah

**Saha Institute of Nuclear Physics, HBNI, Kolkata, India**

S. Baradia, S. Barman[37], S. Bhattacharya, D. Bhowmik, S. Dutta, S. Dutta, B. Gomber[38], M. Maity[37], P. Palit, P.K. Rout, G. Saha, B. Sahu, S. Sarkar

**Indian Institute of Technology Madras, Madras, India**

P.K. Behera, S.C. Behera, P. Kalbhor, J.R. Komaragiri[39], D. Kumar[39], A. Muhammad, L. Panwar[39], R. Pradhan, P.R. Pujahari, A. Sharma, A.K. Sikdar, P.C. Tiwari[39], S. Verma

**Bhabha Atomic Research Centre, Mumbai, India**

K. Naskar[40]

**Tata Institute of Fundamental Research-A, Mumbai, India**

T. Aziz, I. Das, S. Dugad, M. Kumar, G.B. Mohanty, P. Suryadevara

**Tata Institute of Fundamental Research-B, Mumbai, India**

S. Banerjee, R. Chudasama, M. Guchait, S. Karmakar, S. Kumar, G. Majumder, K. Mazumdar, S. Mukherjee, A. Thachayath

JHEP07(2023)077

**National Institute of Science Education and Research, An OCC of Homi Bhabha National Institute, Bhubaneswar, Odisha, India**

S. Bahinipati[41], A.K. Das, C. Kar, P. Mal, T. Mishra, V.K. Muraleedharan Nair Bindhu[42], A. Nayak[42], P. Saha, N. Sur, S.K. Swain, D. Vats[42]

**Indian Institute of Science Education and Research (IISER), Pune, India**

A. Alpana, S. Dube, B. Kansal, A. Laha, S. Pandey, A. Rastogi, S. Sharma

**Isfahan University of Technology, Isfahan, Iran**

H. Bakhshiansohi[43], E. Khazaie, M. Zeinali[44]

**Institute for Research in Fundamental Sciences (IPM), Tehran, Iran**

S. Chenarani[45], S.M. Etesami, M. Khakzad, M. Mohammadi Najafabadi

**University College Dublin, Dublin, Ireland**

M. Grunewald

**INFN Sezione di Bari[a], Università di Bari[b], Politecnico di Bari[c], Bari, Italy**

M. Abbrescia[a,b], R. Aly[a,c,46], C. Aruta[a,b], A. Colaleo[a], D. Creanza[a,c], N. De Filippis[a,c], M. De Palma[a,b], A. Di Florio[a,b], W. Elmetenawee[a,b], F. Errico[a,b], L. Fiore[a], G. Iaselli[a,c], M. Ince[a,b], G. Maggi[a,c], M. Maggi[a], I. Margjeka[a,b], V. Mastrapasqua[a,b], S. My[a,b], S. Nuzzo[a,b], A. Pellecchia[a,b], A. Pompili[a,b], G. Pugliese[a,c], R. Radogna[a], D. Ramos[a], A. Ranieri[a], G. Selvaggi[a,b], L. Silvestris[a], F.M. Simone[a,b], Ü. Sözbilir[a], A. Stamerra[a], R. Venditti[a], P. Verwilligen[a]

**INFN Sezione di Bologna[a], Università di Bologna[b], Bologna, Italy**

G. Abbiendi[a], C. Battilana[a,b], D. Bonacorsi[a,b], L. Borgonovi[a], L. Brigliadori[a], R. Campanini[a,b], P. Capiluppi[a,b], A. Castro[a,b], F.R. Cavallo[a], M. Cuffiani[a,b], G.M. Dallavalle[a], T. Diotalevi[a,b], F. Fabbri[a], A. Fanfani[a,b], P. Giacomelli[a], L. Giommi[a,b], C. Grandi[a], L. Guiducci[a,b], S. Lo Meo[a,47], L. Lunerti[a,b], S. Marcellini[a], G. Masetti[a], F.L. Navarria[a,b], A. Perrotta[a], F. Primavera[a,b], A.M. Rossi[a,b], T. Rovelli[a,b], G.P. Siroli[a,b]

**INFN Sezione di Catania[a], Università di Catania[b], Catania, Italy**

S. Costa[a,b,48], A. Di Mattia[a], R. Potenza[a,b], A. Tricomi[a,b,48], C. Tuve[a,b]

**INFN Sezione di Firenze[a], Università di Firenze[b], Firenze, Italy**

G. Barbagli[a], B. Camaiani[a,b], A. Cassese[a], R. Ceccarelli[a,b], V. Ciulli[a,b], C. Civinini[a], R. D'Alessandro[a,b], E. Focardi[a,b], G. Latino[a,b], P. Lenzi[a,b], M. Lizzo[a,b], M. Meschini[a], S. Paoletti[a], R. Seidita[a,b], G. Sguazzoni[a], L. Viliani[a]

**INFN Laboratori Nazionali di Frascati, Frascati, Italy**

L. Benussi, S. Bianco, S. Meola[22], D. Piccolo

**INFN Sezione di Genova[a], Università di Genova[b], Genova, Italy**

M. Bozzo[a,b], F. Ferro[a], R. Mulargia[a], E. Robutti[a], S. Tosi[a,b]

JHEP07(2023)077

**INFN Sezione di Milano-Bicocca[a], Università di Milano-Bicocca[b], Milano, Italy**

A. Benaglia[a], G. Boldrini[a], F. Brivio[a,b], F. Cetorelli[a,b], F. De Guio[a,b], M.E. Dinardo[a,b], P. Dini[a], S. Gennai[a], A. Ghezzi[a,b], P. Govoni[a,b], L. Guzzi[a,b], M.T. Lucchini[a,b], M. Malberti[a], S. Malvezzi[a], A. Massironi[a], D. Menasce[a], L. Moroni[a], M. Paganoni[a,b], D. Pedrini[a], B.S. Pinolini[a], S. Ragazzi[a,b], N. Redaelli[a], T. Tabarelli de Fatis[a,b], D. Zuolo[a,b]

**INFN Sezione di Napoli[a], Università di Napoli 'Federico II'[b], Napoli, Italy; Università della Basilicata[c], Potenza, Italy; Università G. Marconi[d], Roma, Italy**

S. Buontempo[a], F. Carnevali[a,b], N. Cavallo[a,c], A. De Iorio[a,b], F. Fabozzi[a,c], A.O.M. Iorio[a,b], L. Lista[a,b,49], P. Paolucci[a,22], B. Rossi[a], C. Sciacca[a,b]

**INFN Sezione di Padova[a], Università di Padova[b], Padova, Italy; Università di Trento[c], Trento, Italy**

P. Azzi[a], N. Bacchetta[a,50], D. Bisello[a,b], P. Bortignon[a], A. Bragagnolo[a,b], P. Checchia[a], F. Gasparini[a,b], U. Gasparini[a,b], G. Grosso[a], L. Layer[a,51], E. Lusiani[a], M. Margoni[a,b], G. Maron[a,52], A.T. Meneguzzo[a,b], F. Montecassiano[a], M. Passaseo[a], J. Pazzini[a,b], P. Ronchese[a,b], R. Rossin[a,b], F. Simonetto[a,b], G. Strong[a], M. Tosi[a,b], H. Yarar[a,b], M. Zanetti[a,b], P. Zotto[a,b], A. Zucchetta[a,b]

**INFN Sezione di Pavia[a], Università di Pavia[b], Pavia, Italy**

S. Abu Zeid[a,53], C. Aimè[a,b], A. Braghieri[a], S. Calzaferri[a,b], D. Fiorina[a,b], P. Montagna[a,b], V. Re[a], C. Riccardi[a,b], P. Salvini[a], I. Vai[a], P. Vitulo[a,b]

**INFN Sezione di Perugia[a], Università di Perugia[b], Perugia, Italy**

P. Asenov[a,54], G.M. Bilei[a], D. Ciangottini[a,b], L. Fanò[a,b], M. Magherini[a,b], G. Mantovani[a,b], V. Mariani[a,b], M. Menichelli[a], F. Moscatelli[a,54], A. Piccinelli[a,b], M. Presilla[a,b], A. Rossi[a,b], A. Santocchia[a,b], D. Spiga[a], T. Tedeschi[a,b]

**INFN Sezione di Pisa[a], Università di Pisa[b], Scuola Normale Superiore di Pisa[c], Pisa, Italy; Università di Siena[d], Siena, Italy**

P. Azzurri[a], G. Bagliesi[a], V. Bertacchi[a,c], R. Bhattacharya[a], L. Bianchini[a,b], T. Boccali[a], E. Bossini[a,b], D. Bruschini[a,c], R. Castaldi[a], M.A. Ciocci[a,b], V. D'Amante[a,d], R. Dell'Orso[a], M.R. Di Domenico[a,d], S. Donato[a], A. Giassi[a], F. Ligabue[a,c], G. Mandorli[a,c], D. Matos Figueiredo[a], A. Messineo[a,b], M. Musich[a,b], F. Palla[a], S. Parolia[a,b], G. Ramirez-Sanchez[a,c], A. Rizzi[a,b], G. Rolandi[a,c], S. Roy Chowdhury[a,c], T. Sarkar[a,37], A. Scribano[a], N. Shafiei[a,b], P. Spagnolo[a], R. Tenchini[a], G. Tonelli[a,b], N. Turini[a,d], A. Venturi[a], P.G. Verdini[a]

**INFN Sezione di Roma[a], Sapienza Università di Roma[b], Roma, Italy**

P. Barria[a], M. Campana[a,b], F. Cavallari[a], D. Del Re[a,b], E. Di Marco[a], M. Diemoz[a], E. Longo[a,b], P. Meridiani[a], G. Organtini[a,b], F. Pandolfi[a], R. Paramatti[a,b],

JHEP07(2023)077

C. Quaranta[a,b], S. Rahatlou[a,b], C. Rovelli[a], F. Santanastasio[a,b], L. Soffi[a], R. Tramontano[a,b]

**INFN Sezione di Torino[a], Università di Torino[b], Torino, Italy; Università del Piemonte Orientale[c], Novara, Italy**

N. Amapane[a,b], R. Arcidiacono[a,c], S. Argiro[a,b], M. Arneodo[a,c], N. Bartosik[a], R. Bellan[a,b], A. Bellora[a,b], J. Berenguer Antequera[a,b], C. Biino[a], N. Cartiglia[a], M. Costa[a,b], R. Covarelli[a,b], N. Demaria[a], M. Grippo[a,b], B. Kiani[a,b], F. Legger[a], C. Mariotti[a], S. Maselli[a], A. Mecca[a,b], E. Migliore[a,b], E. Monteil[a,b], M. Monteno[a], M.M. Obertino[a,b], G. Ortona[a], L. Pacher[a,b], N. Pastrone[a], M. Pelliccioni[a], M. Ruspa[a,c], K. Shchelina[a], F. Siviero[a,b], V. Sola[a], A. Solano[a,b], D. Soldi[a,b], A. Staiano[a], M. Tornago[a,b], D. Trocino[a], G. Umoret[a,b], A. Vagnerini[a,b]

**INFN Sezione di Trieste[a], Università di Trieste[b], Trieste, Italy**

S. Belforte[a], V. Candelise[a,b], M. Casarsa[a], F. Cossutti[a], A. Da Rold[a,b], G. Della Ricca[a,b], G. Sorrentino[a,b]

**Kyungpook National University, Daegu, Korea**

S. Dogra, C. Huh, B. Kim, D.H. Kim, G.N. Kim, J. Kim, J. Lee, S.W. Lee, C.S. Moon, Y.D. Oh, S.I. Pak, M.S. Ryu, S. Sekmen, Y.C. Yang

**Chonnam National University, Institute for Universe and Elementary Particles, Kwangju, Korea**

H. Kim, D.H. Moon

**Hanyang University, Seoul, Korea**

E. Asilar, T.J. Kim, J. Park

**Korea University, Seoul, Korea**

S. Cho, S. Choi, S. Han, B. Hong, K. Lee, K.S. Lee, J. Lim, J. Park, S.K. Park, J. Yoo

**Kyung Hee University, Department of Physics, Seoul, Korea**

J. Goh

**Sejong University, Seoul, Korea**

H. S. Kim, Y. Kim, S. Lee

**Seoul National University, Seoul, Korea**

J. Almond, J.H. Bhyun, J. Choi, S. Jeon, W. Jun, J. Kim, J. Kim, J.S. Kim, S. Ko, H. Kwon, H. Lee, J. Lee, S. Lee, B.H. Oh, M. Oh, S.B. Oh, H. Seo, U.K. Yang, I. Yoon

**University of Seoul, Seoul, Korea**

W. Jang, D.Y. Kang, Y. Kang, D. Kim, S. Kim, B. Ko, J.S.H. Lee, Y. Lee, J.A. Merlin, I.C. Park, Y. Roh, D. Song, Watson, I.J., S. Yang

JHEP07(2023)077

**Yonsei University, Department of Physics, Seoul, Korea**
S. Ha, H.D. Yoo

**Sungkyunkwan University, Suwon, Korea**
M. Choi, M.R. Kim, H. Lee, Y. Lee, Y. Lee, I. Yu

**College of Engineering and Technology, American University of the Middle East (AUM), Dasman, Kuwait**
T. Beyrouthy, Y. Maghrbi

**Riga Technical University, Riga, Latvia**
K. Dreimanis, A. Gaile, A. Potrebko, M. Seidel, T. Torims, V. Veckalns

**Vilnius University, Vilnius, Lithuania**
M. Ambrozas, A. Carvalho Antunes De Oliveira, A. Juodagalvis, A. Rinkevicius, G. Tamulaitis

**National Centre for Particle Physics, Universiti Malaya, Kuala Lumpur, Malaysia**
N. Bin Norjoharuddeen, S.Y. Hoh[55], I. Yusuff[55], Z. Zolkapli

**Universidad de Sonora (UNISON), Hermosillo, Mexico**
J.F. Benitez, A. Castaneda Hernandez, H.A. Encinas Acosta, L.G. Gallegos Maríñez, M. León Coello, J.A. Murillo Quijada, A. Sehrawat, L. Valencia Palomo

**Centro de Investigacion y de Estudios Avanzados del IPN, Mexico City, Mexico**
G. Ayala, H. Castilla-Valdez, I. Heredia-De La Cruz[56], R. Lopez-Fernandez, C.A. Mondragon Herrera, D.A. Perez Navarro, A. Sánchez Hernández

**Universidad Iberoamericana, Mexico City, Mexico**
C. Oropeza Barrera, F. Vazquez Valencia

**Benemerita Universidad Autonoma de Puebla, Puebla, Mexico**
I. Pedraza, H.A. Salazar Ibarguen, C. Uribe Estrada

**University of Montenegro, Podgorica, Montenegro**
I. Bubanja, J. Mijuskovic[57], N. Raicevic

**National Centre for Physics, Quaid-I-Azam University, Islamabad, Pakistan**
A. Ahmad, M.I. Asghar, A. Awais, M.I.M. Awan, M. Gul, H.R. Hoorani, W.A. Khan, M. Shoaib, M. Waqas

**AGH University of Science and Technology Faculty of Computer Science, Electronics and Telecommunications, Krakow, Poland**
V. Avati, L. Grzanka, M. Malawski

JHEP07(2023)077

**National Centre for Nuclear Research, Swierk, Poland**

H. Bialkowska, M. Bluj, B. Boimska, M. Górski, M. Kazana, M. Szleper, P. Zalewski

**Institute of Experimental Physics, Faculty of Physics, University of Warsaw, Warsaw, Poland**

K. Bunkowski, K. Doroba, A. Kalinowski, M. Konecki, J. Krolikowski

**Laboratório de Instrumentação e Física Experimental de Partículas, Lisboa, Portugal**

M. Araujo, P. Bargassa, D. Bastos, A. Boletti, P. Faccioli, M. Gallinaro, J. Hollar, N. Leonardo, T. Niknejad, M. Pisano, J. Seixas, O. Toldaiev, J. Varela

**VINCA Institute of Nuclear Sciences, University of Belgrade, Belgrade, Serbia**

P. Adzic[58], M. Dordevic, P. Milenovic, J. Milosevic

**Centro de Investigaciones Energéticas Medioambientales y Tecnológicas (CIEMAT), Madrid, Spain**

M. Aguilar-Benitez, J. Alcaraz Maestre, A. Álvarez Fernández, M. Barrio Luna, Cristina F. Bedoya, C.A. Carrillo Montoya, M. Cepeda, M. Cerrada, N. Colino, B. De La Cruz, A. Delgado Peris, D. Fernández Del Val, J.P. Fernández Ramos, J. Flix, M.C. Fouz, O. Gonzalez Lopez, S. Goy Lopez, J.M. Hernandez, M.I. Josa, J. León Holgado, D. Moran, C. Perez Dengra, A. Pérez-Calero Yzquierdo, J. Puerta Pelayo, I. Redondo, D.D. Redondo Ferrero, L. Romero, S. Sánchez Navas, J. Sastre, L. Urda Gómez, J. Vazquez Escobar, C. Willmott

**Universidad Autónoma de Madrid, Madrid, Spain**

J.F. de Trocóniz

**Universidad de Oviedo, Instituto Universitario de Ciencias y Tecnologías Espaciales de Asturias (ICTEA), Oviedo, Spain**

B. Alvarez Gonzalez, J. Cuevas, J. Fernandez Menendez, S. Folgueras, I. Gonzalez Caballero, J.R. González Fernández, E. Palencia Cortezon, C. Ramón Álvarez, V. Rodríguez Bouza, A. Soto Rodríguez, A. Trapote, C. Vico Villalba

**Instituto de Física de Cantabria (IFCA), CSIC-Universidad de Cantabria, Santander, Spain**

J.A. Brochero Cifuentes, I.J. Cabrillo, A. Calderon, J. Duarte Campderros, M. Fernandez, C. Fernandez Madrazo, A. García Alonso, G. Gomez, C. Lasaosa García, C. Martinez Rivero, P. Martinez Ruiz del Arbol, F. Matorras, P. Matorras Cuevas, J. Piedra Gomez, C. Prieels, A. Ruiz-Jimeno, L. Scodellaro, I. Vila, J.M. Vizan Garcia

JHEP07(2023)077

**University of Colombo, Colombo, Sri Lanka**
M.K. Jayananda, B. Kailasapathy[59], D.U.J. Sonnadara, D.D.C. Wickramarathna

**University of Ruhuna, Department of Physics, Matara, Sri Lanka**
W.G.D. Dharmaratna, K. Liyanage, N. Perera, N. Wickramage

**CERN, European Organization for Nuclear Research, Geneva, Switzerland**
D. Abbaneo, J. Alimena, E. Auffray, G. Auzinger, J. Baechler, P. Baillon†, D. Barney, J. Bendavid, M. Bianco, B. Bilin, A. Bocci, E. Brondolin, C. Caillol, T. Camporesi, G. Cerminara, N. Chernyavskaya, S.S. Chhibra, S. Choudhury, M. Cipriani, L. Cristella, D. d'Enterria, A. Dabrowski, A. David, A. De Roeck, M.M. Defranchis, M. Deile, M. Dobson, M. Dünser, N. Dupont, A. Elliott-Peisert, F. Fallavollita[60], A. Florent, L. Forthomme, G. Franzoni, W. Funk, S. Ghosh, S. Giani, D. Gigi, K. Gill, F. Glege, L. Gouskos, E. Govorkova, M. Haranko, J. Hegeman, V. Innocente, T. James, P. Janot, J. Kaspar, J. Kieseler, N. Kratochwil, S. Laurila, P. Lecoq, E. Leutgeb, A. Lintuluoto, C. Lourenço, B. Maier, L. Malgeri, M. Mannelli, A.C. Marini, F. Meijers, S. Mersi, E. Meschi, F. Moortgat, M. Mulders, S. Orfanelli, L. Orsini, F. Pantaleo, E. Perez, M. Peruzzi, A. Petrilli, G. Petrucciani, A. Pfeiffer, M. Pierini, D. Piparo, M. Pitt, H. Qu, T. Quast, D. Rabady, A. Racz, G. Reales Gutiérrez, M. Rovere, H. Sakulin, J. Salfeld-Nebgen, S. Scarfi, M. Selvaggi, A. Sharma, P. Silva, P. Sphicas[61], A.G. Stahl Leiton, S. Summers, K. Tatar, V.R. Tavolaro, D. Treille, P. Tropea, A. Tsirou, J. Wanczyk[62], K.A. Wozniak, W.D. Zeuner

**Paul Scherrer Institut, Villigen, Switzerland**
L. Caminada[63], A. Ebrahimi, W. Erdmann, R. Horisberger, Q. Ingram, H.C. Kaestli, D. Kotlinski, C. Lange, M. Missiroli[63], L. Noehte[63], T. Rohe

**ETH Zurich - Institute for Particle Physics and Astrophysics (IPA), Zurich, Switzerland**
T.K. Aarrestad, K. Androsov[62], M. Backhaus, P. Berger, A. Calandri, K. Datta, A. De Cosa, G. Dissertori, M. Dittmar, M. Donegà, F. Eble, M. Galli, K. Gedia, F. Glessgen, T.A. Gómez Espinosa, C. Grab, D. Hits, W. Lustermann, A.-M. Lyon, R.A. Manzoni, L. Marchese, C. Martin Perez, A. Mascellani[62], M.T. Meinhard, F. Nessi-Tedaldi, J. Niedziela, F. Pauss, V. Perovic, S. Pigazzini, M.G. Ratti, M. Reichmann, C. Reissel, T. Reitenspiess, B. Ristic, F. Riti, D. Ruini, D.A. Sanz Becerra, J. Steggemann[62], D. Valsecchi[22], R. Wallny

**Universität Zürich, Zurich, Switzerland**
C. Amsler[64], P. Bärtschi, C. Botta, D. Brzhechko, M.F. Canelli, K. Cormier, A. De Wit, R. Del Burgo, J.K. Heikkilä, M. Huwiler, W. Jin, A. Jofrehei, B. Kilminster, S. Leontsinis, S.P. Liechti, A. Macchiolo, P. Meiring, V.M. Mikuni, U. Molinatti, I. Neutelings, A. Reimers, P. Robmann, S. Sanchez Cruz, K. Schweiger, M. Senger, Y. Takahashi

JHEP07(2023)077

**National Central University, Chung-Li, Taiwan**
C. Adloff[65], C.M. Kuo, W. Lin, S.S. Yu

**National Taiwan University (NTU), Taipei, Taiwan**
L. Ceard, Y. Chao, K.F. Chen, P.s. Chen, H. Cheng, W.-S. Hou, Y.y. Li, R.-S. Lu, E. Paganis, A. Psallidas, A. Steen, H.y. Wu, E. Yazgan, P.r. Yu

**Chulalongkorn University, Faculty of Science, Department of Physics, Bangkok, Thailand**
C. Asawatangtrakuldee, N. Srimanobhas

**Çukurova University, Physics Department, Science and Art Faculty, Adana, Turkey**
D. Agyel, F. Boran, Z.S. Demiroglu, F. Dolek, I. Dumanoglu[66], E. Eskut, Y. Guler[67], E. Gurpinar Guler[67], C. Isik, O. Kara, A. Kayis Topaksu, U. Kiminsu, G. Onengut, K. Ozdemir[68], A. Polatoz, A.E. Simsek, B. Tali[69], U.G. Tok, S. Turkcapar, E. Uslan, I.S. Zorbakir

**Middle East Technical University, Physics Department, Ankara, Turkey**
G. Karapinar[70], K. Ocalan[71], M. Yalvac[72]

**Bogazici University, Istanbul, Turkey**
B. Akgun, I.O. Atakisi, E. Gülmez, M. Kaya[73], O. Kaya[74], Ö. Özçelik, S. Tekten[75]

**Istanbul Technical University, Istanbul, Turkey**
A. Cakir, K. Cankocak[66], Y. Komurcu, S. Sen[66]

**Istanbul University, Istanbul, Turkey**
O. Aydilek, S. Cerci[69], B. Hacisahinoglu, I. Hos[76], B. Isildak[77], B. Kaynak, S. Ozkorucuklu, C. Simsek, D. Sunar Cerci[69]

**Institute for Scintillation Materials of National Academy of Science of Ukraine, Kharkiv, Ukraine**
B. Grynyov

**National Science Centre, Kharkiv Institute of Physics and Technology, Kharkiv, Ukraine**
L. Levchuk

**University of Bristol, Bristol, United Kingdom**
D. Anthony, E. Bhal, J.J. Brooke, A. Bundock, E. Clement, D. Cussans, H. Flacher, M. Glowacki, J. Goldstein, G.P. Heath, H.F. Heath, L. Kreczko, B. Krikler, S. Paramesvaran, S. Seif El Nasr-Storey, V.J. Smith, N. Stylianou[78], K. Walkingshaw Pass, R. White

JHEP07(2023)077

**Rutherford Appleton Laboratory, Didcot, United Kingdom**

A.H. Ball, K.W. Bell, A. Belyaev[79], C. Brew, R.M. Brown, D.J.A. Cockerill, C. Cooke, K.V. Ellis, K. Harder, S. Harper, M.-L. Holmberg[80], J. Linacre, K. Manolopoulos, D.M. Newbold, E. Olaiya, D. Petyt, T. Reis, G. Salvi, T. Schuh, C.H. Shepherd-Themistocleous, I.R. Tomalin, T. Williams

**Imperial College, London, United Kingdom**

R. Bainbridge, P. Bloch, S. Bonomally, J. Borg, S. Breeze, C.E. Brown, O. Buchmuller, V. Cacchio, V. Cepaitis, G.S. Chahal[81], D. Colling, J.S. Dancu, P. Dauncey, G. Davies, J. Davies, M. Della Negra, S. Fayer, G. Fedi, G. Hall, M.H. Hassanshahi, A. Howard, G. Iles, J. Langford, L. Lyons, A.-M. Magnan, S. Malik, A. Martelli, M. Mieskolainen, D.G. Monk, J. Nash[82], M. Pesaresi, B.C. Radburn-Smith, D.M. Raymond, A. Richards, A. Rose, E. Scott, C. Seez, A. Shtipliyski, R. Shukla, A. Tapper, K. Uchida, G.P. Uttley, L.H. Vage, T. Virdee[22], M. Vojinovic, N. Wardle, S.N. Webb, D. Winterbottom

**Brunel University, Uxbridge, United Kingdom**

K. Coldham, J.E. Cole, A. Khan, P. Kyberd, I.D. Reid

**Baylor University, Waco, Texas, USA**

S. Abdullin, A. Brinkerhoff, B. Caraway, J. Dittmann, K. Hatakeyama, A.R. Kanuganti, B. McMaster, M. Saunders, S. Sawant, C. Sutantawibul, J. Wilson

**Catholic University of America, Washington, DC, USA**

R. Bartek, A. Dominguez, R. Uniyal, A.M. Vargas Hernandez

**The University of Alabama, Tuscaloosa, Alabama, USA**

A. Buccilli, S.I. Cooper, D. Di Croce, S.V. Gleyzer, C. Henderson, C.U. Perez, P. Rumerio[83], C. West

**Boston University, Boston, Massachusetts, USA**

A. Akpinar, A. Albert, D. Arcaro, C. Cosby, Z. Demiragli, C. Erice, E. Fontanesi, D. Gastler, S. May, J. Rohlf, K. Salyer, D. Sperka, D. Spitzbart, I. Suarez, A. Tsatsos, S. Yuan

**Brown University, Providence, Rhode Island, USA**

G. Benelli, B. Burkle, X. Coubez[24], D. Cutts, M. Hadley, U. Heintz, J.M. Hogan[84], T. Kwon, G. Landsberg, K.T. Lau, D. Li, J. Luo, M. Narain, N. Pervan, S. Sagir[85], F. Simpson, E. Usai, W.Y. Wong, X. Yan, D. Yu, W. Zhang

**University of California, Davis, Davis, California, USA**

J. Bonilla, C. Brainerd, R. Breedon, M. Calderon De La Barca Sanchez, M. Chertok, J. Conway, P.T. Cox, R. Erbacher, G. Haza, F. Jensen, O. Kukral, G. Mocellin, M. Mulhearn, D. Pellett, B. Regnery, D. Taylor, Y. Yao, F. Zhang

JHEP07(2023)077

**University of California, Los Angeles, California, USA**
M. Bachtis, R. Cousins, A. Datta, D. Hamilton, J. Hauser, M. Ignatenko, M.A. Iqbal, T. Lam, E. Manca, W.A. Nash, S. Regnard, D. Saltzberg, B. Stone, V. Valuev

**University of California, Riverside, Riverside, California, USA**
Y. Chen, R. Clare, J.W. Gary, M. Gordon, G. Hanson, G. Karapostoli, O.R. Long, N. Manganelli, W. Si, S. Wimpenny

**University of California, San Diego, La Jolla, California, USA**
J.G. Branson, P. Chang, S. Cittolin, S. Cooperstein, D. Diaz, J. Duarte, R. Gerosa, L. Giannini, J. Guiang, R. Kansal, V. Krutelyov, R. Lee, J. Letts, M. Masciovecchio, F. Mokhtar, M. Pieri, B.V. Sathia Narayanan, V. Sharma, M. Tadel, F. Würthwein, Y. Xiang, A. Yagil

**University of California, Santa Barbara - Department of Physics, Santa Barbara, California, USA**
N. Amin, C. Campagnari, M. Citron, G. Collura, A. Dorsett, V. Dutta, J. Incandela, M. Kilpatrick, J. Kim, A.J. Li, B. Marsh, P. Masterson, H. Mei, M. Oshiro, M. Quinnan, J. Richman, U. Sarica, R. Schmitz, F. Setti, J. Sheplock, P. Siddireddy, D. Stuart, S. Wang

**California Institute of Technology, Pasadena, California, USA**
A. Bornheim, O. Cerri, I. Dutta, J.M. Lawhorn, N. Lu, J. Mao, H.B. Newman, T. Q. Nguyen, M. Spiropulu, J.R. Vlimant, C. Wang, S. Xie, R.Y. Zhu

**Carnegie Mellon University, Pittsburgh, Pennsylvania, USA**
J. Alison, S. An, M.B. Andrews, P. Bryant, T. Ferguson, A. Harilal, C. Liu, T. Mudholkar, S. Murthy, M. Paulini, A. Roberts, A. Sanchez, W. Terrill

**University of Colorado Boulder, Boulder, Colorado, USA**
J.P. Cumalat, W.T. Ford, A. Hassani, G. Karathanasis, E. MacDonald, F. Marini, R. Patel, A. Perloff, C. Savard, N. Schonbeck, K. Stenson, K.A. Ulmer, S.R. Wagner, N. Zipper

**Cornell University, Ithaca, New York, USA**
J. Alexander, S. Bright-Thonney, X. Chen, D.J. Cranshaw, J. Fan, X. Fan, D. Gadkari, S. Hogan, J. Monroy, J.R. Patterson, D. Quach, J. Reichert, M. Reid, A. Ryd, J. Thom, P. Wittich, R. Zou

**Fermi National Accelerator Laboratory, Batavia, Illinois, USA**
M. Albrow, M. Alyari, G. Apollinari, A. Apresyan, L.A.T. Bauerdick, D. Berry, J. Berryhill, P.C. Bhat, K. Burkett, J.N. Butler, A. Canepa, G.B. Cerati, H.W.K. Cheung, F. Chlebana, K.F. Di Petrillo, J. Dickinson, V.D. Elvira, Y. Feng, J. Freeman, A. Gandrakota, Z. Gecse, L. Gray, D. Green, S. Grünendahl,

JHEP07(2023)077

O. Gutsche, R.M. Harris, R. Heller, T.C. Herwig, J. Hirschauer, L. Horyn, B. Jayatilaka, S. Jindariani, M. Johnson, U. Joshi, T. Klijnsma, B. Klima, K.H.M. Kwok, S. Lammel, D. Lincoln, R. Lipton, T. Liu, C. Madrid, K. Maeshima, C. Mantilla, D. Mason, P. McBride, P. Merkel, S. Mrenna, S. Nahn, J. Ngadiuba, D. Noonan, V. Papadimitriou, N. Pastika, K. Pedro, C. Pena[86], F. Ravera, A. Reinsvold Hall[87], L. Ristori, E. Sexton-Kennedy, N. Smith, A. Soha, L. Spiegel, J. Strait, L. Taylor, S. Tkaczyk, N.V. Tran, L. Uplegger, E.W. Vaandering, H.A. Weber, I. Zoi

**University of Florida, Gainesville, Florida, USA**

P. Avery, D. Bourilkov, L. Cadamuro, V. Cherepanov, R.D. Field, D. Guerrero, M. Kim, E. Koenig, J. Konigsberg, A. Korytov, K.H. Lo, K. Matchev, N. Menendez, G. Mitselmakher, A. Muthirakalayil Madhu, N. Rawal, D. Rosenzweig, S. Rosenzweig, K. Shi, J. Wang, Z. Wu

**Florida State University, Tallahassee, Florida, USA**

T. Adams, A. Askew, R. Habibullah, V. Hagopian, R. Khurana, T. Kolberg, G. Martinez, H. Prosper, C. Schiber, O. Viazlo, R. Yohay, J. Zhang

**Florida Institute of Technology, Melbourne, Florida, USA**

M.M. Baarmand, S. Butalla, T. Elkafrawy[53], M. Hohlmann, R. Kumar Verma, M. Rahmani, F. Yumiceva

**University of Illinois at Chicago (UIC), Chicago, Illinois, USA**

M.R. Adams, H. Becerril Gonzalez, R. Cavanaugh, S. Dittmer, O. Evdokimov, C.E. Gerber, D.J. Hofman, D. S. Lemos, A.H. Merrit, C. Mills, G. Oh, T. Roy, S. Rudrabhatla, M.B. Tonjes, N. Varelas, X. Wang, Z. Ye, J. Yoo

**The University of Iowa, Iowa City, Iowa, USA**

M. Alhusseini, K. Dilsiz[88], L. Emediato, R.P. Gandrajula, G. Karaman, O.K. Köseyan, J.-P. Merlo, A. Mestvirishvili[89], J. Nachtman, O. Neogi, H. Ogul[90], Y. Onel, A. Penzo, C. Snyder, E. Tiras[91]

**Johns Hopkins University, Baltimore, Maryland, USA**

O. Amram, B. Blumenfeld, L. Corcodilos, J. Davis, A.V. Gritsan, L. Kang, S. Kyriacou, P. Maksimovic, J. Roskes, S. Sekhar, M. Swartz, T.Á. Vámi

**The University of Kansas, Lawrence, Kansas, USA**

A. Abreu, L.F. Alcerro Alcerro, J. Anguiano, P. Baringer, A. Bean, Z. Flowers, T. Isidori, S. Khalil, J. King, G. Krintiras, M. Lazarovits, C. Le Mahieu, C. Lindsey, J. Marquez, N. Minafra, M. Murray, M. Nickel, C. Rogan, C. Royon, R. Salvatico, S. Sanders, E. Schmitz, C. Smith, Q. Wang, J. Williams, G. Wilson

JHEP07(2023)077

**Kansas State University, Manhattan, Kansas, USA**

B. Allmond, S. Duric, R. Gujju Gurunadha, A. Ivanov, K. Kaadze, D. Kim, Y. Maravin, T. Mitchell, A. Modak, K. Nam, J. Natoli, D. Roy

**Lawrence Livermore National Laboratory, Livermore, California, USA**

F. Rebassoo, D. Wright

**University of Maryland, College Park, Maryland, USA**

E. Adams, A. Baden, O. Baron, A. Belloni, A. Bethani, S.C. Eno, N.J. Hadley, S. Jabeen, R.G. Kellogg, T. Koeth, Y. Lai, S. Lascio, A.C. Mignerey, S. Nabili, C. Palmer, C. Papageorgakis, L. Wang, K. Wong

**Massachusetts Institute of Technology, Cambridge, Massachusetts, USA**

D. Abercrombie, R. Bi, W. Busza, I.A. Cali, Y. Chen, M. D'Alfonso, J. Eysermans, C. Freer, G. Gomez-Ceballos, M. Goncharov, P. Harris, M. Hu, D. Kovalskyi, J. Krupa, Y.-J. Lee, K. Long, C. Mironov, C. Paus, D. Rankin, C. Roland, G. Roland, Z. Shi, G.S.F. Stephans, J. Wang, Z. Wang, B. Wyslouch

**University of Minnesota, Minneapolis, Minnesota, USA**

R.M. Chatterjee, B. Crossman, A. Evans, J. Hiltbrand, Sh. Jain, B.M. Joshi, C. Kapsiak, M. Krohn, Y. Kubota, J. Mans, M. Revering, R. Rusack, R. Saradhy, N. Schroeder, N. Strobbe, M.A. Wadud

**University of Mississippi, Oxford, Mississippi, USA**

L.M. Cremaldi

**University of Nebraska-Lincoln, Lincoln, Nebraska, USA**

K. Bloom, M. Bryson, D.R. Claes, C. Fangmeier, L. Finco, F. Golf, C. Joo, I. Kravchenko, I. Reed, J.E. Siado, G.R. Snow†, W. Tabb, A. Wightman, F. Yan, A.G. Zecchinelli

**State University of New York at Buffalo, Buffalo, New York, USA**

G. Agarwal, H. Bandyopadhyay, L. Hay, I. Iashvili, A. Kharchilava, C. McLean, M. Morris, D. Nguyen, J. Pekkanen, S. Rappoccio, A. Williams

**Northeastern University, Boston, Massachusetts, USA**

G. Alverson, E. Barberis, Y. Haddad, Y. Han, A. Krishna, J. Li, J. Lidrych, G. Madigan, B. Marzocchi, D.M. Morse, V. Nguyen, T. Orimoto, A. Parker, L. Skinnari, A. Tishelman-Charny, T. Wamorkar, B. Wang, A. Wisecarver, D. Wood

**Northwestern University, Evanston, Illinois, USA**

S. Bhattacharya, J. Bueghly, Z. Chen, A. Gilbert, T. Gunter, K.A. Hahn, Y. Liu, N. Odell, M.H. Schmitt, M. Velasco

JHEP07(2023)077

**University of Notre Dame, Notre Dame, Indiana, USA**
R. Band, R. Bucci, S. Castells, M. Cremonesi, A. Das, R. Goldouzian, M. Hildreth, K. Hurtado Anampa, C. Jessop, K. Lannon, J. Lawrence, N. Loukas, L. Lutton, J. Mariano, N. Marinelli, I. Mcalister, T. McCauley, C. Mcgrady, K. Mohrman, C. Moore, Y. Musienko[13], H. Nelson, R. Ruchti, A. Townsend, M. Wayne, H. Yockey, M. Zarucki, L. Zygala

**The Ohio State University, Columbus, Ohio, USA**
B. Bylsma, M. Carrigan, L.S. Durkin, B. Francis, C. Hill, A. Lesauvage, M. Nunez Ornelas, K. Wei, B.L. Winer, B. R. Yates

**Princeton University, Princeton, New Jersey, USA**
F.M. Addesa, B. Bonham, P. Das, G. Dezoort, P. Elmer, A. Frankenthal, B. Greenberg, N. Haubrich, S. Higginbotham, A. Kalogeropoulos, G. Kopp, S. Kwan, D. Lange, D. Marlow, K. Mei, I. Ojalvo, J. Olsen, D. Stickland, C. Tully

**University of Puerto Rico, Mayaguez, Puerto Rico, USA**
S. Malik, S. Norberg

**Purdue University, West Lafayette, Indiana, USA**
A.S. Bakshi, V.E. Barnes, R. Chawla, S. Das, L. Gutay, M. Jones, A.W. Jung, D. Kondratyev, A.M. Koshy, M. Liu, G. Negro, N. Neumeister, G. Paspalaki, S. Piperov, A. Purohit, J.F. Schulte, M. Stojanovic, J. Thieman, F. Wang, R. Xiao, W. Xie

**Purdue University Northwest, Hammond, Indiana, USA**
J. Dolen, N. Parashar

**Rice University, Houston, Texas, USA**
D. Acosta, A. Baty, T. Carnahan, M. Decaro, S. Dildick, K.M. Ecklund, P.J. Fernández Manteca, S. Freed, P. Gardner, F.J.M. Geurts, A. Kumar, W. Li, B.P. Padley, R. Redjimi, J. Rotter, W. Shi, S. Yang, E. Yigitbasi, L. Zhang[92], Y. Zhang, X. Zuo

**University of Rochester, Rochester, New York, USA**
A. Bodek, P. de Barbaro, R. Demina, J.L. Dulemba, C. Fallon, T. Ferbel, M. Galanti, A. Garcia-Bellido, O. Hindrichs, A. Khukhunaishvili, E. Ranken, R. Taus, G.P. Van Onsem

**The Rockefeller University, New York, New York, USA**
K. Goulianos

**Rutgers, The State University of New Jersey, Piscataway, New Jersey, USA**
B. Chiarito, J.P. Chou, Y. Gershtein, E. Halkiadakis, A. Hart, M. Heindl, D. Jaroslawski, O. Karacheban[26], I. Laflotte, A. Lath, R. Montalvo, K. Nash,

JHEP07(2023)077

M. Osherson, S. Salur, S. Schnetzer, S. Somalwar, R. Stone, S.A. Thayil, S. Thomas, H. Wang

**University of Tennessee, Knoxville, Tennessee, USA**

H. Acharya, A.G. Delannoy, S. Fiorendi, T. Holmes, E. Nibigira, S. Spanier

**Texas A&M University, College Station, Texas, USA**

O. Bouhali[93], M. Dalchenko, A. Delgado, R. Eusebi, J. Gilmore, T. Huang, T. Kamon[94], H. Kim, S. Luo, S. Malhotra, R. Mueller, D. Overton, D. Rathjens, A. Safonov

**Texas Tech University, Lubbock, Texas, USA**

N. Akchurin, J. Damgov, V. Hegde, K. Lamichhane, S.W. Lee, T. Mengke, S. Muthumuni, T. Peltola, I. Volobouev, Z. Wang, A. Whitbeck

**Vanderbilt University, Nashville, Tennessee, USA**

E. Appelt, S. Greene, A. Gurrola, W. Johns, A. Melo, F. Romeo, P. Sheldon, S. Tuo, J. Velkovska, J. Viinikainen

**University of Virginia, Charlottesville, Virginia, USA**

B. Cardwell, B. Cox, G. Cummings, J. Hakala, R. Hirosky, M. Joyce, A. Ledovskoy, A. Li, C. Neu, C.E. Perez Lara, B. Tannenwald

**Wayne State University, Detroit, Michigan, USA**

P.E. Karchin, N. Poudyal

**University of Wisconsin - Madison, Madison, Wisconsin, USA**

S. Banerjee, K. Black, T. Bose, S. Dasu, I. De Bruyn, P. Everaerts, C. Galloni, H. He, M. Herndon, A. Herve, C.K. Koraka, A. Lanaro, A. Loeliger, R. Loveless, J. Madhusudanan Sreekala, A. Mallampalli, A. Mohammadi, S. Mondal, G. Parida, D. Pinna, A. Savin, V. Shang, V. Sharma, W.H. Smith, D. Teague, H.F. Tsoi, W. Vetens

**Authors affiliated with an institute or an international laboratory covered by a cooperation agreement with CERN**

S. Afanasiev, V. Andreev, Yu. Andreev, T. Aushev, M. Azarkin, A. Babaev, A. Belyaev, V. Blinov[95], E. Boos, V. Borshch, D. Budkouski, V. Bunichev, O. Bychkova, V. Chekhovsky, R. Chistov[95], M. Danilov[95], A. Dermenev, T. Dimova[95], I. Dremin, M. Dubinin[86], L. Dudko, V. Epshteyn, A. Ershov, G. Gavrilov, V. Gavrilov, S. Gninenko, V. Golovtcov, N. Golubev, I. Golutvin, I. Gorbunov, A. Gribushin, V. Ivanchenko, Y. Ivanov, V. Kachanov, L. Kardapoltsev[95], V. Karjavine, A. Karneyeu, V. Kim[95], M. Kirakosyan, D. Kirpichnikov, M. Kirsanov, V. Klyukhin, D. Konstantinov, V. Korenkov, A. Kozyrev[95], N. Krasnikov, E. Kuznetsova[96], A. Lanev, P. Levchenko, A. Litomin, N. Lychkovskaya, V. Makarenko, A. Malakhov, V. Matveev[95], V. Murzin, A. Nikitenko[97],



JHEP07(2023)077

S. Obraztsov, V. Okhotnikov, A. Oskin, I. Ovtin[95], V. Palichik, P. Parygin, V. Perelygin, M. Perfilov, G. Pivovarov, S. Polikarpov[95], V. Popov, O. Radchenko[95], M. Savina, V. Savrin, V. Shalaev, S. Shmatov, S. Shulha, Y. Skovpen[95], S. Slabospitskii, V. Smirnov, D. Sosnov, A. Stepennov, V. Sulimov, E. Tcherniaev, A. Terkulov, O. Teryaev, I. Tlisova, M. Toms, A. Toropin, L. Uvarov, A. Uzunian, E. Vlasov, P. Volkov, A. Vorobyev, N. Voytishin, B.S. Yuldashev[98], A. Zarubin, I. Zhizhin, A. Zhokin

[†] *Deceased*
[1] *Also at Yerevan State University, Yerevan, Armenia*
[2] *Also at TU Wien, Vienna, Austria*
[3] *Also at Institute of Basic and Applied Sciences, Faculty of Engineering, Arab Academy for Science, Technology and Maritime Transport, Alexandria, Egypt*
[4] *Also at Université Libre de Bruxelles, Bruxelles, Belgium*
[5] *Also at Universidade Estadual de Campinas, Campinas, Brazil*
[6] *Also at Federal University of Rio Grande do Sul, Porto Alegre, Brazil*
[7] *Also at UFMS, Nova Andradina, Brazil*
[8] *Also at The University of the State of Amazonas, Manaus, Brazil*
[9] *Also at University of Chinese Academy of Sciences, Beijing, China*
[10] *Also at Nanjing Normal University Department of Physics, Nanjing, China*
[11] *Now at The University of Iowa, Iowa City, Iowa, USA*
[12] *Also at University of Chinese Academy of Sciences, Beijing, China*
[13] *Also at an institute or an international laboratory covered by a cooperation agreement with CERN*
[14] *Also at Cairo University, Cairo, Egypt*
[15] *Also at Suez University, Suez, Egypt*
[16] *Now at British University in Egypt, Cairo, Egypt*
[17] *Also at Purdue University, West Lafayette, Indiana, USA*
[18] *Also at Université de Haute Alsace, Mulhouse, France*
[19] *Also at Department of Physics, Tsinghua University, Beijing, China*
[20] *Also at Tbilisi State University, Tbilisi, Georgia*
[21] *Also at Erzincan Binali Yildirim University, Erzincan, Turkey*
[22] *Also at CERN, European Organization for Nuclear Research, Geneva, Switzerland*
[23] *Also at University of Hamburg, Hamburg, Germany*
[24] *Also at RWTH Aachen University, III. Physikalisches Institut A, Aachen, Germany*
[25] *Also at Isfahan University of Technology, Isfahan, Iran*
[26] *Also at Brandenburg University of Technology, Cottbus, Germany*
[27] *Also at Forschungszentrum Jülich, Juelich, Germany*
[28] *Also at Physics Department, Faculty of Science, Assiut University, Assiut, Egypt*
[29] *Also at Karoly Robert Campus, MATE Institute of Technology, Gyongyos, Hungary*
[30] *Also at Wigner Research Centre for Physics, Budapest, Hungary*
[31] *Also at Institute of Physics, University of Debrecen, Debrecen, Hungary*
[32] *Also at Institute of Nuclear Research ATOMKI, Debrecen, Hungary*
[33] *Now at Universitatea Babes-Bolyai - Facultatea de Fizica, Cluj-Napoca, Romania*
[34] *Also at Faculty of Informatics, University of Debrecen, Debrecen, Hungary*
[35] *Also at Punjab Agricultural University, Ludhiana, India*
[36] *Also at UPES - University of Petroleum and Energy Studies, Dehradun, India*
[37] *Also at University of Visva-Bharati, Santiniketan, India*
[38] *Also at University of Hyderabad, Hyderabad, India*
[39] *Also at Indian Institute of Science (IISc), Bangalore, India*
[40] *Also at Indian Institute of Technology (IIT), Mumbai, India*
[41] *Also at IIT Bhubaneswar, Bhubaneswar, India*

JHEP07(2023)077

[42] Also at Institute of Physics, Bhubaneswar, India
[43] Also at Deutsches Elektronen-Synchrotron, Hamburg, Germany
[44] Also at Sharif University of Technology, Tehran, Iran
[45] Also at Department of Physics, University of Science and Technology of Mazandaran, Behshahr, Iran
[46] Also at Helwan University, Cairo, Egypt
[47] Also at Italian National Agency for New Technologies, Energy and Sustainable Economic Development, Bologna, Italy
[48] Also at Centro Siciliano di Fisica Nucleare e di Struttura Della Materia, Catania, Italy
[49] Also at Scuola Superiore Meridionale, Università di Napoli 'Federico II', Napoli, Italy
[50] Also at Fermi National Accelerator Laboratory, Batavia, Illinois, USA
[51] Also at Università di Napoli 'Federico II', Napoli, Italy
[52] Also at Laboratori Nazionali di Legnaro dell'INFN, Legnaro, Italy
[53] Also at Ain Shams University, Cairo, Egypt
[54] Also at Consiglio Nazionale delle Ricerche - Istituto Officina dei Materiali, Perugia, Italy
[55] Also at Department of Applied Physics, Faculty of Science and Technology, Universiti Kebangsaan Malaysia, Bangi, Malaysia
[56] Also at Consejo Nacional de Ciencia y Tecnología, Mexico City, Mexico
[57] Also at IRFU, CEA, Université Paris-Saclay, Gif-sur-Yvette, France
[58] Also at Faculty of Physics, University of Belgrade, Belgrade, Serbia
[59] Also at Trincomalee Campus, Eastern University, Sri Lanka, Nilaveli, Sri Lanka
[60] Also at INFN Sezione di Pavia, Università di Pavia, Pavia, Italy
[61] Also at National and Kapodistrian University of Athens, Athens, Greece
[62] Also at Ecole Polytechnique Fédérale Lausanne, Lausanne, Switzerland
[63] Also at Universität Zürich, Zurich, Switzerland
[64] Also at Stefan Meyer Institute for Subatomic Physics, Vienna, Austria
[65] Also at Laboratoire d'Annecy-le-Vieux de Physique des Particules, IN2P3-CNRS, Annecy-le-Vieux, France
[66] Also at Near East University, Research Center of Experimental Health Science, Mersin, Turkey
[67] Also at Konya Technical University, Konya, Turkey
[68] Also at Izmir Bakircay University, Izmir, Turkey
[69] Also at Adiyaman University, Adiyaman, Turkey
[70] Also at Istanbul Gedik University, Istanbul, Turkey
[71] Also at Necmettin Erbakan University, Konya, Turkey
[72] Also at Bozok Universitetesi Rektörlügü, Yozgat, Turkey
[73] Also at Marmara University, Istanbul, Turkey
[74] Also at Milli Savunma University, Istanbul, Turkey
[75] Also at Kafkas University, Kars, Turkey
[76] Also at Istanbul University - Cerrahpasa, Faculty of Engineering, Istanbul, Turkey
[77] Also at Yildiz Technical University, Istanbul, Turkey
[78] Also at Vrije Universiteit Brussel, Brussel, Belgium
[79] Also at School of Physics and Astronomy, University of Southampton, Southampton, United Kingdom
[80] Also at University of Bristol, Bristol, United Kingdom
[81] Also at IPPP Durham University, Durham, United Kingdom
[82] Also at Monash University, Faculty of Science, Clayton, Australia
[83] Also at Università di Torino, Torino, Italy
[84] Also at Bethel University, St. Paul, Minnesota, USA
[85] Also at Karamanoğlu Mehmetbey University, Karaman, Turkey
[86] Also at California Institute of Technology, Pasadena, California, USA
[87] Also at United States Naval Academy, Annapolis, Maryland, USA
[88] Also at Bingol University, Bingol, Turkey
[89] Also at Georgian Technical University, Tbilisi, Georgia
[90] Also at Sinop University, Sinop, Turkey

JHEP07(2023)077

[91] *Also at Erciyes University, Kayseri, Turkey*
[92] *Also at Institute of Modern Physics and Key Laboratory of Nuclear Physics and Ion-beam Application (MOE) - Fudan University, Shanghai, China*
[93] *Also at Texas A&M University at Qatar, Doha, Qatar*
[94] *Also at Kyungpook National University, Daegu, Korea*
[95] *Also at another institute or international laboratory covered by a cooperation agreement with CERN*
[96] *Now at University of Florida, Gainesville, Florida, USA*
[97] *Also at Imperial College, London, United Kingdom*
[98] *Also at Institute of Nuclear Physics of the Uzbekistan Academy of Sciences, Tashkent, Uzbekistan*

JHEP07(2023)077